A Wind Tunnel Facility for the Evaluation of a Land-based Gas Turbine Diffuser-collector

Nihar R. Samal

Thesis submitted to the faculty of the Virginia Polytechnic Institute and State University in partial fulfillment of the requirements for the degree of

Master of Science
in
Mechanical Engineering

Wing Ng, Committee Chair
Todd K. Lowe
Clinton L. Dancey

December 7th , 2011
Blacksburg, VA

Keywords: Annular diffuser, Diffuser-Collector, Exhaust hood, Pressure recovery, Stereo-PIV)

A Wind Tunnel Facility for the Evaluation of a Land-based Gas Turbine Diffuser-collector

Nihar R. Samal

ABSTRACT

A subsonic wind tunnel facility was built and tested as part of a base line test investigating flow within a diffuser-collector. Facility controls allowed the quarter scale model to match both Reynolds number and Mach number. Mass averaged conditions at the diffuser inlet during testing were determined as 1.939×10^6 for Reynolds number based upon diffuser inlet hydraulic diameter, and 0.418 for Mach number. A flow conditioning section prior to test section contained several interchangeable sections. Flow conditioning components were used to create flow characteristic of that leaving the last stage of a land-based gas turbine. The diffuser-collector subsystem was evaluated through the use of wall static pressure measurements, a variety of probe traverse measurements, and Stereo-PIV. Flow within the collector and diffuser were determined to be heavily dependent upon the collector geometry. PIV measurements showed the development of two large counter rotating vortices within the collector. Each symmetric vortex grew and shifted according to the collector geometry while creating complex regions of flow. Pressure recovery within the diffuser was in range of 0.47 to 0.78, and would drop to 0.52 at the collector exit. The drop in pressure recovery was presumed to be a combination of inefficient diffusion in the collector and losses due to the vortices. The baseline test was found to be successful in terms of facility design, and determining the critical flow phenomena. Further testing and experimentation are necessary to evaluate specific details of the collector geometry's effect upon the pressure recovery and flow development.

Acknowledgements

Many thanks to Dr. Wing Ng, Dr. Todd Lowe, and Dr. Clint Dancey for serving on my committee, and for their continuous assistance throughout the project. I'd really like to thank Dr. Ng for giving me the opportunity to work on this project and for his constant support over the year. Thanks to Dr. Lowe for his guidance and assistance with the Stereo-PIV measurements. Special thanks to my mentor Stephen Guillot at Techsburg. His incredibly vast knowledge and our continuous discussions were critical to the progression of this project. Thanks to Ulrich Stang, and Hans Hamm from Solar Turbines for sponsoring the project and for their valuable feedback.

Without the support of the Techsburg staff and Dr. Ng's and Dr. Lowe's research group's this project wouldn't have been possible. Thank you to Matt Langford, Jon Fleming, Sarah Tweedie, and Zach Boor for assistance with programming, design, assembly, and of course troubleshooting. Thank you to Tamara Murray for taking care of the massive amounts of paperwork dealt with during the project. Thanks to Gary Dudding, Greg Whittaker, and the entire machine shop for modifying and creating any necessary wind tunnel components

The endless support from parents, Babru and Jayashree, was a driving factor in my success with this project. And of course thank you to all my friends and particularly my girlfriend, Shivani for supporting me and my stomach throughout whatever we do. I greatly appreciate all the help that I've gotten throughout the past year, and hope I too can provide the immense amount of support each of you gave me.

Table of Contents

Index of Figures

Index of Equations

Nomenclature

Acronyms

CAD	Computer Aided Design
CCD	Charge-coupled device
CFD	Computational Fluid Dynamics
DAQ	Data acquisition
DEHS	Di(2-ethylhexyl) sebacate
ID	Inner diameter
OD	Outer diameter
PIV	Particle Image Velocimetry
SLS	Selective Laser Sintering

Greek

γ	Ratio of specific heats
α	Kinetic energy flux velocity profile parameter
β	Perforated plate grid porosity
δ	Uncertainty
σ	Standard deviation
ρ	Density
μ	Kinematic viscosity

Variables

A	Annular area
A_B	Blocked annular area
B	Blockage at diffuser inlet
C	Turbulence intensity constant
C_p	Pressure Recovery based upon diffuser inlet and collector exit
C_{pc}	Local Pressure Recovery based upon diffuser inlet
d_e	Effective grid dimension for perforated plate
D	Hole diameter of perforated plate
D_h	Hydraulic diameter of diffuser inlet
h^*	Dimensionless annular height ($Hub = 0\,, Case\ = 1.0$)
L	Axial length from diffuser inlet to diffuser exit
Ma	Mach Number
N	Number of data samples
Nu	Nusselt Number
P_s	Static pressure
P_s^*	Static pressure coefficient
P_t	Total pressure
P_t^*	Total pressure coefficient
Re	Reynolds Number
t	Plate thickness for perforated plate

Tu	Turbulence intensity
u	Local axial velocity
U	Maximum axial velocity in annulus
V	Arbitrary velocity from SPIV data
z	Axial distance downstream

Subscripts

1	Upstream location
2	Downstream location
$exit$	Measured at collector exit
$inlet$	Measured at diffuser inlet
$meas$	Measured value taken at any arbitrary position

Superscripts

$\bar{}$	Time averaged value
$\bar{\bar{}}$	Mass averaged value calculated from time averaged values

Chapter 1 – Introduction

1.1: Background of the Diffuser-Collector

Geometrically a diffuser is a component with an increasing area ratio over an axial distance. Diffuser geometry can vary in length, angle, as well as cross-section. The three most common cross-sections found within diffusers are rectangular, conical, and annular. The increasing area ratio of the diffuser is commonly used for two main purposes: reduction in velocity for subsonic flow, and increase of static pressure. In turbomachinery applications the diffuser has been used for its static pressure rise before exhausting flow to atmosphere. By placing the diffusers after the last stage of the turbine, energy within the fluid that would have been otherwise wasted is used to reduce backpressure on the turbine. Reduction in the turbine backpressure increases the work output and therefore can improve stage efficiency.

The use of a collector is typical for land based turbine applications where proper ventilation of the exhaust gases is necessary. The enclosed structure of the collector is commonly combined with the exhaust diffuser, and involves a 90º turn. While flow of exhaust diffusers has been widely researched, the understanding of flow within a combined diffuser-collector subsystem is still not well known.

1.2: Previous Research

As mentioned previously a large variety of research has been previously done on exhaust diffusers. Typically research involves investigation on the effects of various flow parameters upon diffuser performance. The combined diffuser-collector subsystem is a relatively new topic of research and still has many unanswered questions.

1.2.1: Diffuser Research

Sovran and Klomp 1965 could be regarded as the most widespread diffuser paper. Pressure recovery data was obtained for over a hundred diffusers of varying geometry using uniform inlet flow with small blockage, and no swirl distribution. From this large amount of data a family of curves for general diffuser design was created. These plots are commonly referenced to determine the most efficient diffuser design based upon prescribed area ratio, or axial length.

While Sovran and Klomp's paper was extremely beneficial to diffuser design, it did not account for the varying flow parameters typically seen at the diffuser inlet. Later diffuser research would study the effect of turbulence intensity, swirl distribution, blockage, Mach number along with a number of other parameters.

Japikse and Pampreen 1978 conducted a series of experiments testing variable swirl and inlet Mach number upon an automotive gas turbine. The test rig included an inter-stage diffuser, exhaust diffuser and double discharge collector. Inlet conditions of the one-third scaled exhaust diffuser would match blockage and Reynolds number. Pressure probes and flow visualization were used to characterize the flow. Data showed a slight decline in diffuser recovery at higher swirl angles with larger declines at higher Mach numbers.

Hoffman 1981 studied the effect of free stream turbulence on diffuser performance. Pressure and hot wire measurements were taken within a small scale diffuser using a small blockage parameter. Variation in turbulence levels, using equally spaced rods, showed increasing pressure recovery with increasing turbulence levels. It was concluded that eddies perpendicular to the

flow and parallel to diverging walls transmitted turbulent energy efficiently and delayed separation.

In 2000, Ubertini and Desideri studied the effect of struts on flow phenomena and exhaust diffuser performance. A 35% scaled down model was tested with inlet conditions mimicking the swirl distribution and wakes produced by last rotor stage of the turbine. Pressure measurements along with hot film measurements were used to identify differences in flow structures. It was found that struts located within the diffuser would reduce pressure recovery and increase pressure losses. Diffusion was decreased due to reduction in area, and the wakes created by the struts.

Many other papers have conducted research similar to the papers above and continue to do so In 1998 Japikse and Baines wrote a book summarizing important discoveries, and diffuser design criteria for conical, annular, and rectilinear diffusers.

1.2.2: Diffuser-Collector Research

Research of combined diffuser-collector system was less of a commonality in the past, but is becoming a topic of importance. Several papers mentioned below discuss the effect of a collector or exhaust hood on the performance the diffuser as well as subsystem performance.

Finzel and Casey studied the sensitivity of particular exhaust hood geometry on the pressure recovery of the exhaust subsystem [Finzel 2011]. A Mach number of 0.5 and matching radial swirl distribution were used on the scaled model to mimic operating conditions. Pressure taps along the diffuser walls, and traversed measurements at the diffuser inlet and diffuser outlet were taken to characterize the flow. Results showed that restricted areas within the exhaust hood flow path strongly influenced the diffuser flow and reduced pressure recovery.

The study of two geometrically different exhaust hoods on diffuser performance was done experimentally by Yoon and Stanislaus for validation of numerical simulations [Yoon 2011]. A 10% scale diffuser model was tested using a model turbine at representative inlet Mach number, and approximate Reynolds number. Several pressure taps along with multiple traverse locations were used to characterize pressure recovery. By analyzing the three dimensional exhaust hood geometry increased diffuser recovery was achieved.

Most recently, Bernier conducted experimental and computational research investigating the effect of collector geometry upon the exhaust diffuser performance [Bernier 2011]. A small scale diffuser-collector subsystem was tested at Mach 0.2 using a uniform velocity profile and unknown blockage. Total pressure measurements at the exit of the collector revealed the presence of two large counter rotating vortices predicted in the computational model. It was found that changes of the collector geometry would reduce the strength of the vortices while also improving the diffuser-collector efficiency.

This study intended to create a facility where detailed characteristics of production diffuser-collector flow field could be observed in order to improve the exhaust system performance.

Chapter 2 - Wind Tunnel Facility Design

Experimental testing for this project was done at the Techsburg Wind Tunnel Facility located in Christiansburg, VA. The Techsburg facility is an intermittent blowdown tunnel capable of adapting to a large variety of experimental setups. The facility initially consisted of several components that included a compressor, air storage tanks, a control valve, a settling chamber, a butterfly valve, and an exhaust silencer. A geometrically similar subscale model of the diffuser-collector section was designed along with a flow conditioning section to work with the prior wind tunnel components. An optical table was designed as well to house the necessary PIV equipment used during the project. Details on the blow down facility, the experimental flow path, and the optical table design can be found below.

2.1: Blow Down Facility

The Techsburg facility takes advantage of using a blowdown configuration as mentioned before. Using a blowdown configuration allows for the ability to test at variable conditions such as high mass flow rate or high Mach number with quick start up times. An overview of the entire facility is shown in Figure 2–1.

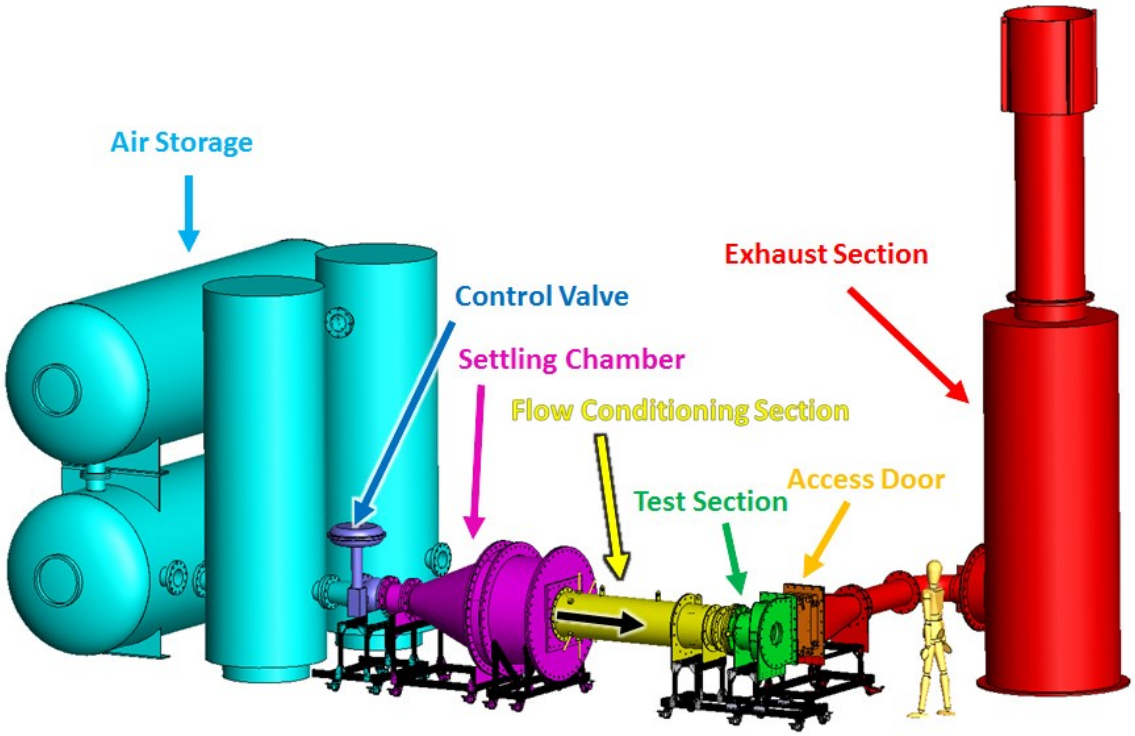

Figure 2–1: A perspective view of the wind tunnel facility CAD model shows facility overview. Components have been colored for identification. A mannequin standing 5ft 9inches is shown next to the facility for scale.

Tanks used to hold compressed air are shown in light blue. The particular configuration at Techsburg used a Kaeser CSD-100S rotary screw type compressor to bring air in large storage tanks up to 200 psi. Two 1550 gallon vertical tanks and two 7600 gallon tanks give a facility total storage capacity of 10,700 gallons of air.

A control valve, shown in dark blue, was used to vary the rate of the air leaving the tanks. Flow leaving the control valve entered the settling chamber, shown in pink, which was used to create clean uniform flow for the rest of the facility. Uniform flow then entered the flow

conditioning section, shown in yellow, which would create the characteristic flow necessary for our test section. Flow within the test section, shown in green, was measured by taking pressure data along with PIV data. An access duct, shown in orange, allowed for easy entree to the test section and would house part of the optics used during the PIV measurements. Parts shown in red represent the exhaust section. General facility components are described in the sections below, while components critical to the test section are described later in Chapter 3.

2.1.1: Control Valve

A short adapter was added to the facility in order to attach the existing 12" Fisher Vee-Ball Control Valve to the 8'' exit of the storage tanks. Variation in the rate at which the control valve opens plays an important factor in tunnel conditions. Once the control valve has been initially opened, the pressure in the storage tank quickly drops. To keep consistent conditions the control valve must be opened in a manner proportional to the pressure drop in the tanks. A Siemens Moore 353 Process Automation Controller, shown in Figure 2–2b, was used to control this specific rate which will be discussed further in Chapter 4.1. The controller can also be used to check variables such as tank pressure, control valve opening percentage, wind tunnel run time, and it also includes an emergency shutoff mechanism.

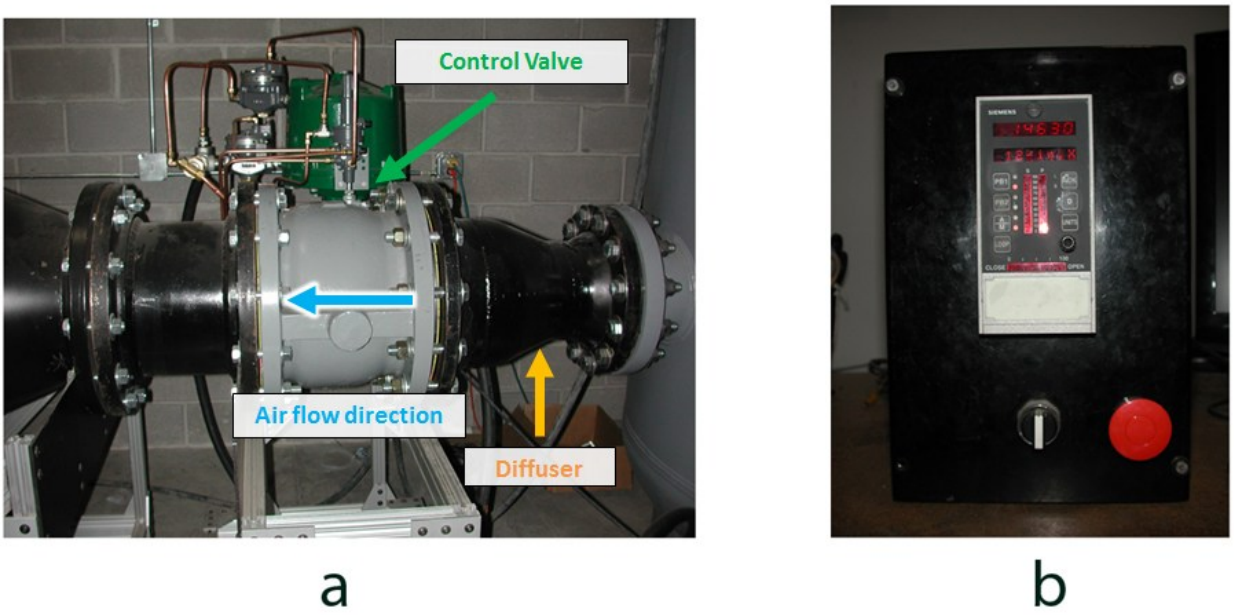

Figure 2–2: a) A short diffuser section connects the control valve to the pressurized tanks b) A Siemens controller was used to regulate the release of pressurized air from the storage tanks

2.1.2: Settling Chamber

Once the control valve opens, highly turbulent and non-uniform air from the storage tanks rushes into the settling chamber. The settling chamber, shown in Figure 2–3, consists of several different mechanisms that are used to make the erratic incoming flow uniform.

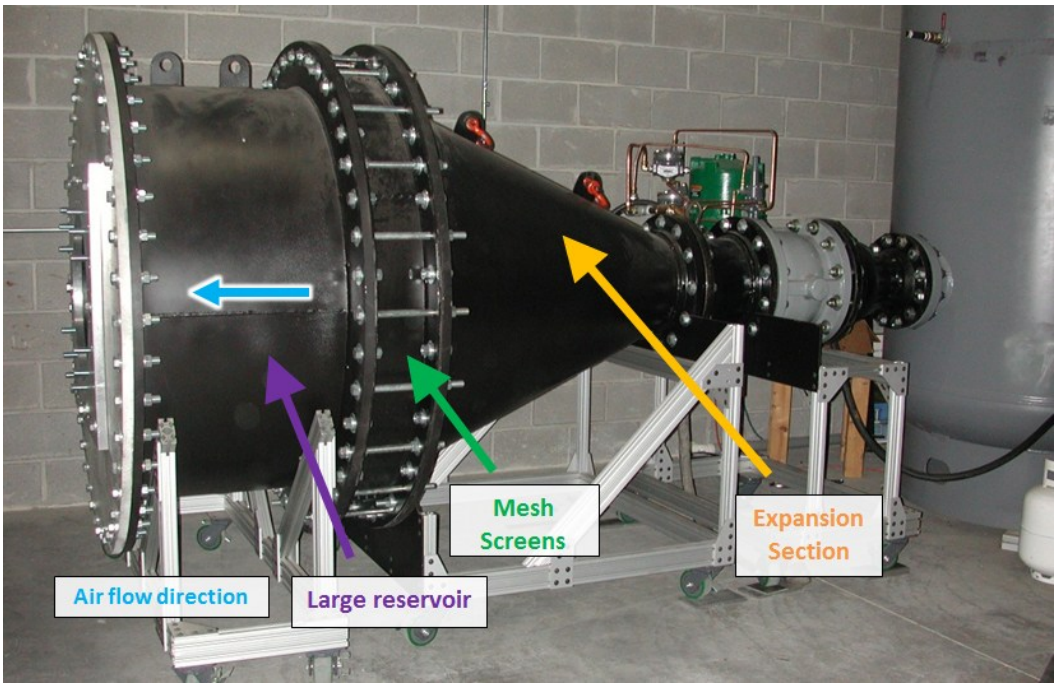

Figure 2–3: An external view of the settling chambers major components

The first portion of the settling chamber is an expansion section where the flow rapidly expands from a 12.25'' ID to a 45.2'' ID over a 42'' axial distance. Near the end of the expansion section, the flow encounters a pyramid shaped flow spreader shown in Figure 2–4. The flow spreader is a made of several perforated sheet metal pieces welded together in the shape of a pyramid, where the pyramid point is pointing upstream. This pyramid point helps to break up the core of the oncoming fluid, and the perforated holes assist in diffusing the fluid further.

Figure 2–4: Looking upstream into the settling chamber towards the inlet of the expansion section, the geometry of flow spreader can be more clearly visualized

The next section is a short axial section which contains ring shaped spacers. The spacers allow for a variable number of screens to be bolted in radially. To remove any potential separation caused by the expansion section, mesh screens are used because of their ease of use and low cost [Pope 1999]. The screens create more uniform flow and can reduce turbulence intensity by breaking larger scale eddies [Prandtl 1933]. The screen also creates small scale eddies on the order of the wire diameter which dissipate quickly. This setup took advantage of two rigid mesh screens of wire diameter 0.03'' spaced at approximately 4''apart.

The last section of settling chamber is a large reservoir containing a bell-mouth contraction. The clean flow is near stagnant in the large reservoir section and enters a long 19.5'' ID duct through the contraction. This long duct ultimately leads to the flow conditioning section, and is a primary component used for seeding the flow for PIV. This large contraction was designed by Matt Langford and evaluated using the CFD software ADPAC to minimize separation due small curvature radii. Details of the flow conditioning section are discussed in Chapter 2.3, and modifications of the large 19.5'' OD duct for PIV are discussed in Chapter 2.4.

2.1.3: Butterfly Valve & Exhaust Flow path

Flow from the test section was known to exit from a rectangular cross-section. An exhaust flow path made of carbon steel sheet metal components, shown in Figure 2–5, was designed to take the flow exiting from the test section to the silencer where it would exhaust to atmosphere.

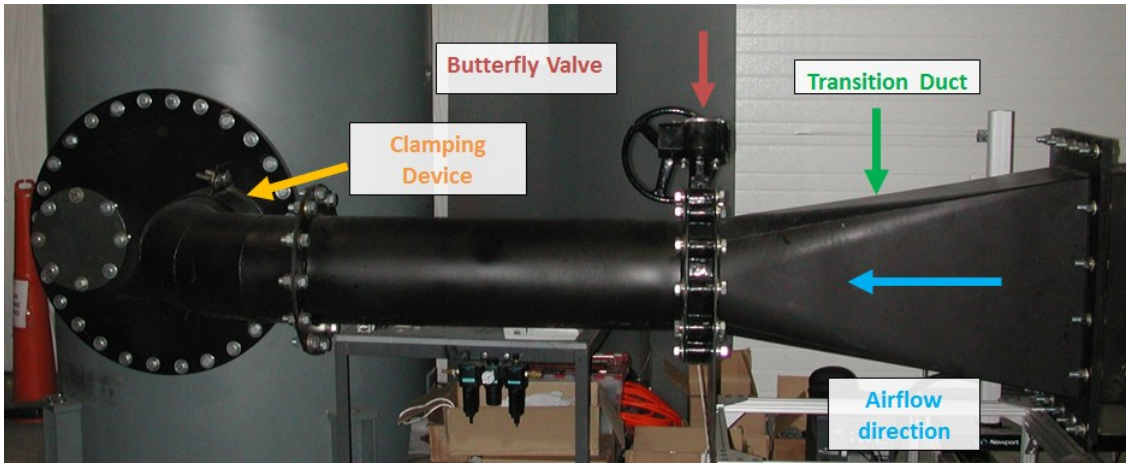

Figure 2–5: The exhaust section contains several simple but critical components for the facility

A butterfly valve was also used in this flow path in order to control the backpressure for the experimental setup. The combination of the butterfly valve position and the control valve settings allowed the total pressure and the flow rate to be set independently making it possible to match both the Mach number and Reynolds number in the scaled facility. Details of the butterfly valve settings used are discussed in the Chapter 4.1. To take advantage of the butterfly valve, a transition duct was used to go from a rectangular cross section to a circular cross section. Flow exiting from the butterfly valve would continue through a straight circular pipe, and an elbow was used to connect to the flange of the silencer. The connection of the elbow to the silencer flange used a C-shaped clamping device for sealing. Using a clamping device was important as it would allow a variable length of the elbow to slide into the silencer. Varying the length of the facility was a key feature as defined by the flow conditioning section, details can be found in Chapter 2.3.

2.1.4: Silencer

High speed flow exhausting to atmosphere has been known to exhibit large amounts of noise. The Techsburg facility uses a Burgess-Manning SDA-44-2 Silencer to dampen the noise created by the exiting flow. This particular model is specifically designed to withstand high impact forces, such as those seen in a blow down facility. The silencer, shown in Figure 2–6, uses several layers of moisture resistant mineral wool for acoustic control while a diffuser within the plenum controls the pressure expansion of the flow.

Figure 2–6: The exhaust section of the facility connects to the silencer which muffles noise created by the exiting flow

2.2: Scaling & Design of the Diffuser-Collector Section

To study the aerodynamics of a collector-diffuser section for a gas turbine a scaled research rig was designed to be tested in the Techsburg wind tunnel facility. A solid model provided by Solar Turbine contained the full scale geometry of the collector-diffuser section with all its minute complexities, but was simplified to only the necessary flow features for the Techsburg experimental model as shown in Figure 2–7. The experimental model matched the Mach number and Reynolds number, but the geometry and surface roughness were scaled to one fourth the original size.

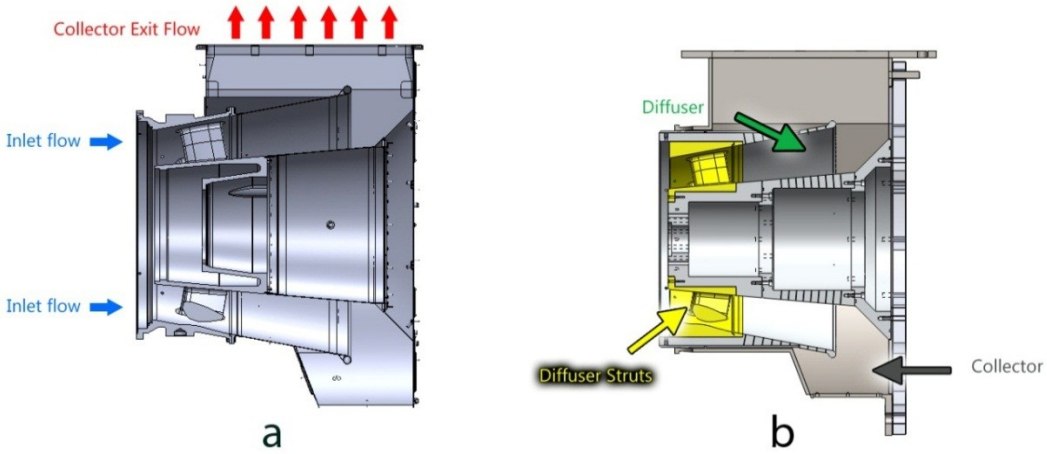

Figure 2–7: a) CAD of Solar Turbine Collector Diffuser Section b) CAD of Techsburg Quarter scale experimental model

2.2.1: Scaling & Material Selection

The scaling of the experimental model was determined to be one quarter after analysis of the possible flow conditions at the Techsburg facility. The flow path OD of the scaled down diffuser inlet was approximately 11.92''. Mach number at the inlet of the diffuser and Reynolds number would match the flow of the full scale Solar Turbine collector diffuser section. The Mach number being matched is 0.420, while the Reynolds number based upon hydraulic diameter is matched to be 1.94×10^6 .

Sandcasting of the production diffuser-collector section led to rough parts with a surface roughness in the range of 150 to 250 micro inches. Scaling the roughness by a quarter led to the desired range of 37.5 to 62.5 micro inches for the experimental test section. Aluminum 6061 was chosen for the majority of critical components upon comparing accuracy of the manufacturing methods, material properties, and cost. Carbon steel sheet metal was used for the collector due to its large size, and to simplify the manufacturing of this already complex component. Parts within the diffuser-collector section were also anodized or painted with a flat black to minimize reflections during PIV measurements.

2.2.2: Simplifications & Modifications of Diffuser-Collector Section

The diffuser-collector section was geometrically simplified for the test facility, only the essential flow features were kept. A large portion of the production model included mounting points on the case and hubs which were changed based upon the upstream and downstream components in the experimental facility. Heat expansion joints found in the production model were also ignored as they were deemed unnecessary for the experimental test conditions.

To obtain various flow quantities for the analysis of the diffuser-collector section, the model was modified to accommodate instrumentation. Holes and small windows along with other minor changes were put into the diffuser-collector section to provide locations for static pressure taps, traverse measurements, as well as PIV measurements. The entire back plane of the collector was made of a 1.25'' Clear Cast Acrylic in order to have optical access for the cameras during PIV. Details of these specific changes can be found in Appendix A.

2.2.3: Critical Diffuser-Collector Features

As discussed in the previous section, the test article is a simplified version of the Solar Turbine model. This section discusses the details for geometry in the test article that were critical in the effort to keep the test article representative of the production hardware. Several of these critical features could also be studied in future tests.

One of the important flow features in the test section is the area where the flow in the diffuser annulus dumps into the collector. The collector wall is angled with respect to the horizontal which is shown in Figure 2–8.

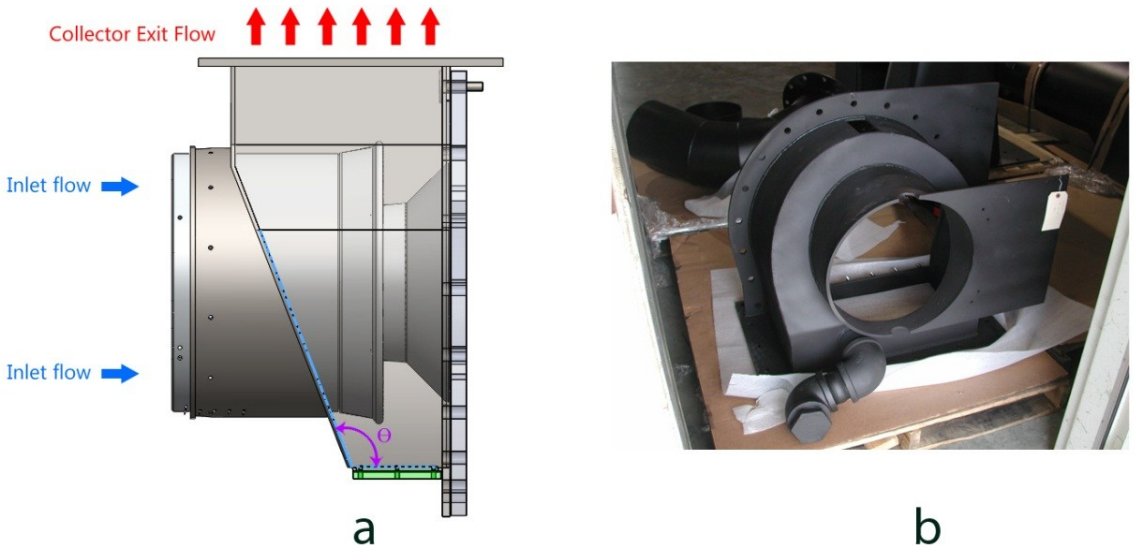

Figure 2–8: a) The collector angle to be changed in future studies. b) The collector shell to be replaced in order to change the angle.

The angle theta, shown in purple, was assumed to be a critical geometric feature that influences the development of secondary flow in the collector. In order to investigate how this angle may change the secondary flow, the collector angle needed to be changed for future tests. Sheet metal was used to manufacture the entire collector because it is a cost effective yet rigid material. When a new angle would be studied the entire collector shell would be replaced.

Another geometric feature that requires future investigation is the bleed pipe in the collector section. The collector shell needed the ability to connect an external and internal elbow as specified by Solar Turbine. The internal elbow will be used in the future to study the effect of bleed flow on the secondary flow in the collector. Various attachments to the bleed pipe inside the collector could also be used for stress analysis of the collector rear wall plate due to the bleed flow. Figure 2–9 illustrates an example of how the internal elbow could be connected to the collector shell. Note that the internal elbow is not part of the production model, and would only be used to examine the flow.

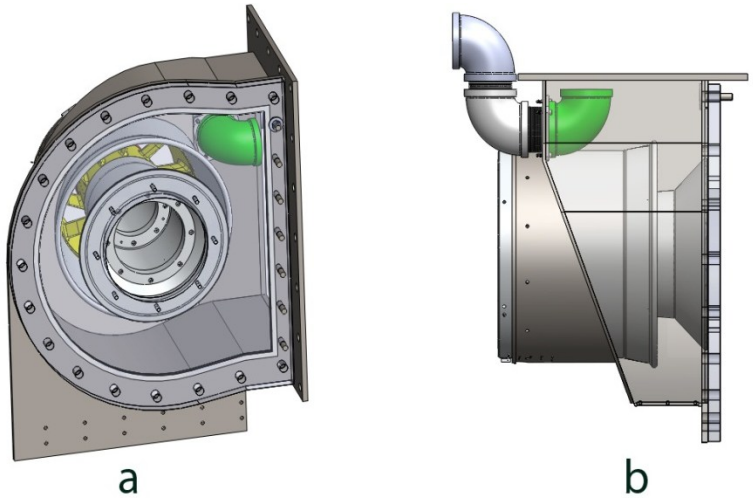

Figure 2–9: a) An isometric view showing the internal elbow in green connected using a small flange b) A top view, show the external and internal elbows in their planned orientation

At the inlet plane of the diffuser, small structural members are used to connect the diffuser case and diffuser hub. In order to study the effect that these structural components have on diffuser performance, the diffuser case allows for interchangeable diffuser struts as shown in Figure 2–10. The specific struts used during testing were designed by Solar Turbines to act as a de-swirler for the expected swirl distribution seen at the diffuser inlet.

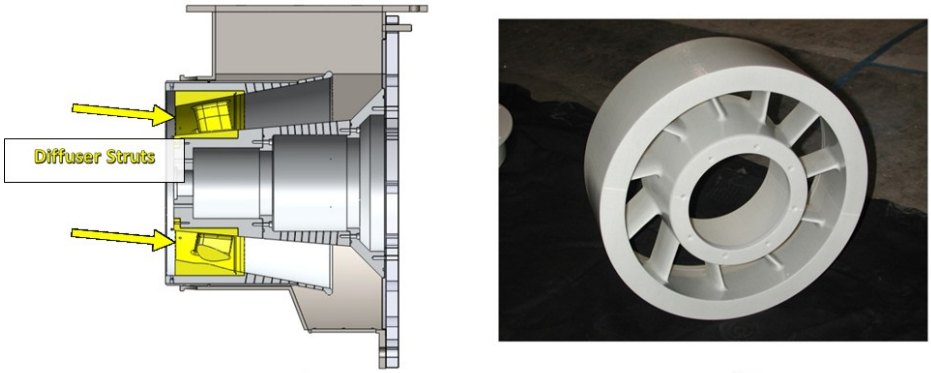

Figure 2–10: a) The diffuser struts shown in yellow can slide into the diffuser case and hub b) Struts made of the Glass filled Nylon SLS material exhibit both lean and sweep

Small struts of various designs could be manufactured separately and slid into the diffuser casing to be secured by several bolts. Rapid prototyping materials were used due to quick turnaround time, and low cost for highly complex geometries. Specifically, glass-filled Nylon SLS was chosen due to manufacturing limitations and its flexural and tensile strength. The surface roughness for this SLS part was approximately 260 micro inches Ra, which is much larger than the scaled roughness range of 37.5 to 62.5 micro inches. The SLS part was sanded down in order to get the roughness within the desired range.

In an attempt to keep concentricity between the many diffuser parts, mating surfaces were used between all diffuser parts. One part features a revolved extrusion and overlaps onto the next part creating a tight fit. These mating surfaces are also used in the flow conditioning section of the experimental setup to avoid misalignment issues. An example of these mating surfaces is shown below in Figure 2–11

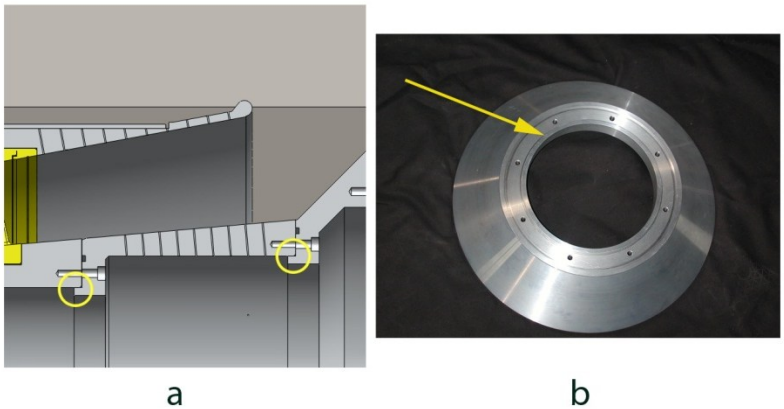

Figure 2–11: a) Yellow circles indicated the mating surfaces used b) A top view of a diffuser component with an arrow pointing at the mating surface that points upstream

2.3: Flow Conditioning Section

To match the flow conditions seen by the real diffuser-collector section, components such as a turbulence grid, swirl vanes, and a small contraction were used. Geometry for the flow conditioning section was provided by Hans Hamm Jr. at Solar Turbines who used CFD along with other analysis tools for evaluation. A section view of the CAD model showing all the flow conditioning components used to modify the inlet flow can be seen in Figure 2–12.

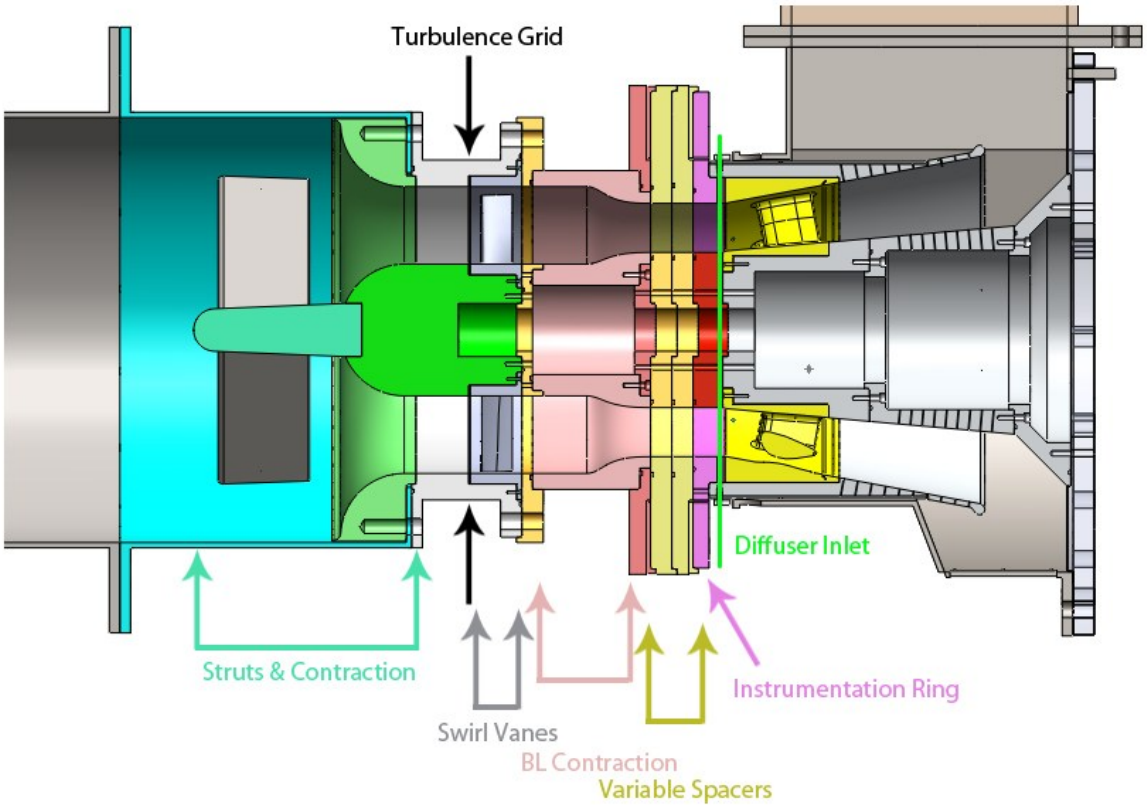

Figure 2–12: An overview of the flow conditioning components

2.3.1: Large Contraction & Structural Members

Figure 2–13 shows a side view of the large struts, the nose cone, and the large contraction. .Four large struts were used to support the center body components. The large struts have a smooth airfoil-like shape and were placed in a large annulus to minimize any impact on the flow. A smooth nose cone attached the structural members to the center body, and was followed in the flow path by a large contraction.

The large contraction takes the flow from the large area and smoothly accelerates the flow into an annulus. This contraction has an area ratio of approximately 2.78.

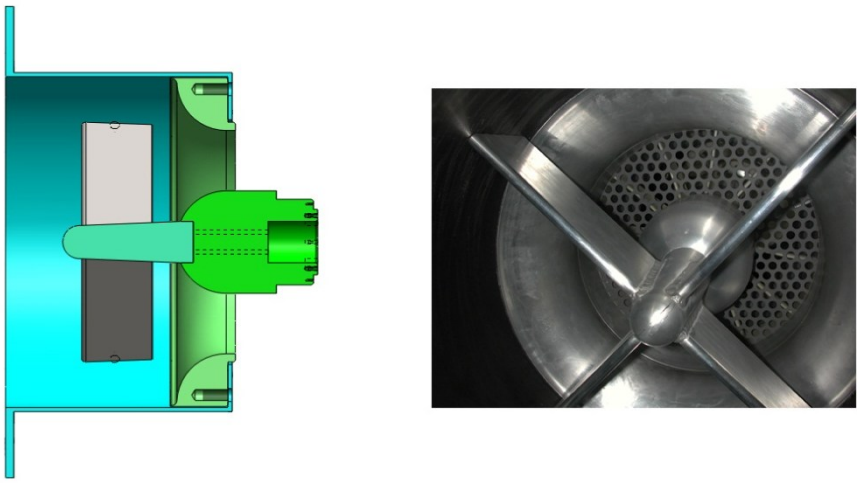

Figure 2–13: a) Large gray structural members provide support for the green center body piece b) A perspective view of the air foil like struts

2.3.2: Turbulence Grid

To obtain the desired turbulence level downstream a 1/16th inch carbon steel porous plate was put into the flow. A variety of porosities can be used to generate different turbulence intensities at the exit of the flow path contraction. The hole size and estimated turbulence intensity was determined using Equations 2-1, 2-2, and 2-3. Roach's 1987 paper uses several assumptions to relate a porous plate to a turbulence grid by creating an effective diameter. Experimental data for a variety of porous plates was used to obtain the relationships in Equation 2-1, and Equation 2-2. As distance away from the grid increases, turbulence intensity decreases in a proportional manner. The grid currently uses a ½'' hole staggered pattern with a spacing of 11/16'' and was estimated to create turbulence intensities around 6.3% at the diffuser inlet. An incompressible assumption was used in Equation 2-4 to determine a 4% turbulence intensity value to account for the area contraction.

$$\frac{d_e}{D} = \frac{1}{\beta^{\frac{1}{2}}} - 1 \qquad \text{Equation 2-1}$$

$$C = 0.77\left(\frac{t}{D}\right)^{-0.14} \qquad \text{Equation 2-2}$$

$$Tu = C\left(\frac{z}{d_e}\right)^{-\left(\frac{5}{7}\right)} \qquad \text{Equation 2-3}$$

$$Tu_2 = Tu_1\left(\frac{A_1}{A_2}\right) \qquad \text{Equation 2-4}$$

The turbulence grid was placed upstream of the swirl vanes to minimize its impact on the swirl distribution and boundary layer profile. The facility design allows for the turbulence grid to

move further downstream if higher turbulence intensities are necessary. Figure 2–14 shows a downstream of view of the flow path with the turbulence grid in black.

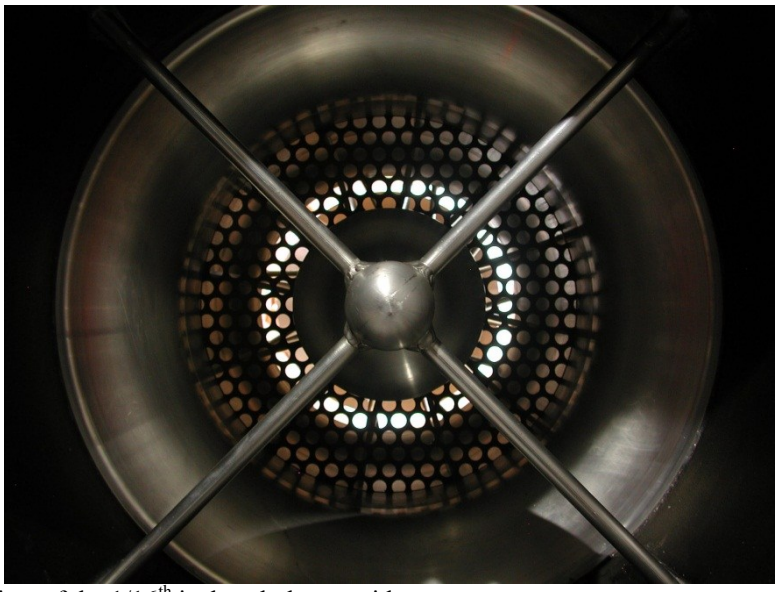

Figure 2–14: A front view of the 1/16th inch turbulence grid

2.3.3: Inlet Swirl Vanes

Similar to the diffuser struts, the inlet swirl vanes were designed to be interchangeable as well. Swirl vanes were used in attempt to mimic the swirling flow exiting the last rotor stage in the turbine. Different swirl distributions occur based upon the turbine operating point. The swirl vanes used during testing were designed to mimic the distribution produced when the turbine was operating at 100% speed. By allowing the vanes to be interchangeable the effect of the turbine operating speed on the secondary flow could be studied in the future. Glass Filled Nylon SLS rapid prototyping material was chosen as it allowed for quick reproduction of structurally stable complex shapes. Figure 2–15 shows a perspective view of the swirl vanes produced for the project.

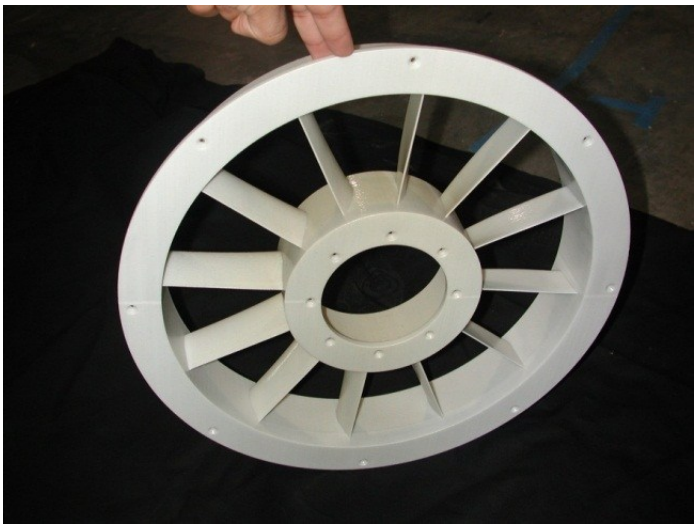

Figure 2–15: A perspective view shows the trailing edge of swirl vanes that induce the required swirl distribution

2.3.4: Boundary Layer Contraction

To achieve the necessary boundary layer profile at the inlet of the diffuser a boundary layer contraction was used. Modification of the flow path geometry changes the pressure distribution and therefore affects the boundary layer as well as the velocity distribution [Bell 1988]. The smooth spline contraction goes from an outer diameter of 13.5 inches to 11.925 inches, and an inner diameter of 6.2 inches to 7.3 inches. If the boundary layer achieved using the 1.617 area ratio is not optimal, the flow conditioning section can be reassembled using another contraction. Figure 2–16 shows the CAD model of the boundary layer contraction and a perspective view of the contraction during facility assembly.

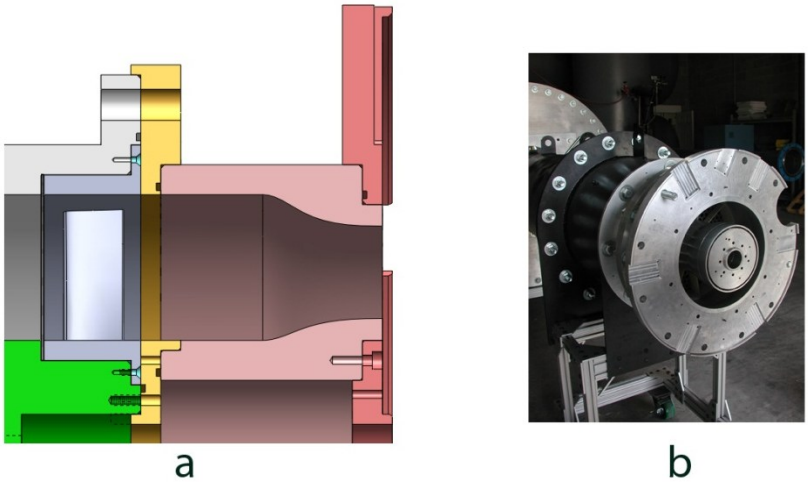

Figure 2–16: a) CFD was used to determine the contraction geometry shown here in pink b) A perspective view shows the contractions during the assembly of the facility

2.3.5: Variable Spacing Length

One inch incremental spacers were manufactured to fit between the boundary layer contraction and the instrumentation ring. These spacers allow for further axial length to vary the boundary layer thickness and hence the amount of blockage desired. Without any spacers the minimum axial distance from the boundary layer contraction to the diffuser inlet plane was 1.25 in. With the variable spacers included distances between 1.25in and 4.25 in could be achieved. Figure 2–17 shows the variable spacers on the hub and case in the CAD model. During testing no spacers were used, to achieve minimum distance from the boundary layer contraction to the diffuser inlet.

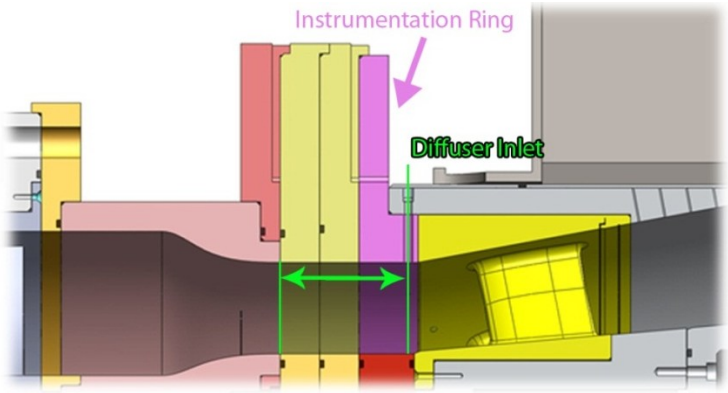

Figure 2–17: 1 inch incremental spacers, shown in gold for the hub and yellow for the case, can be used to vary the distance from the Boundary layer contraction to the instrumentation ring

2.4: PIV Seeding & Access Duct

Since PIV was a major part of this project, seeding needed to be entered into the flow path. Seed was introduced into the facility as far upstream as possible using seeding wands in order to uniformly distribute the seed. A LaVision Aerosol seeder used pressurized air to push DEHS, Di(2-ethylhexyl) sebacate, into the seeding wands. DEHS was chosen for the seed because of it was a colorless liquid based seed with a fast time response that LaVision seeder had been designed to use [Ragni 2011]. The seeding wands are hollow ¾'' OD stainless steel tubes with a 3/32'' linear hole pattern. The small hole pattern allowed the seed to exit at a velocity similar to the flow in the duct. Due to significant swirl in flow in the test section, the positioning of the seeding wand could affect the seeding uniformity and placement. Eight seeding wands positions were positioned 8.5'' inches from the bellmouth contraction located in the settling chamber. The eight positions allowed variability in where the seeding entered the flow, and hence the distribution of seed in the test section. Figure 2–18 shows the seeding wand positions relative to the settling chamber.

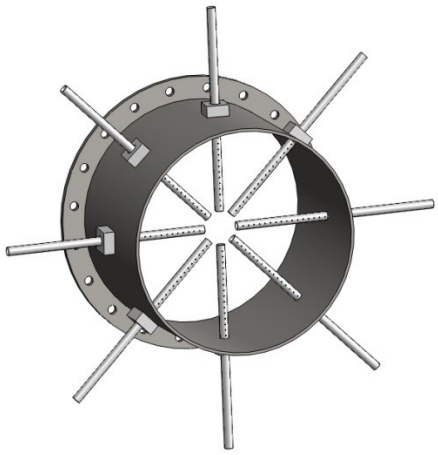

Figure 2–18: A section view of the CAD model shows the many seeding wand positions allowed for a single position or several positions for the seed to enter the flow.

As PIV uses seed to illuminate the flow, seed tends to build up on the surfaces of the wind tunnel. In this facility the majority of seed entering the flow would impact the rear wall of the collector, which was the PIV field of view. In order to keep a clear field of view, an access door was added just downstream of the collector. A large access door allowed for the test section to be cleaned whenever seed build up was in issue in the facility. This access duct also contained four holes downstream of the door. Two acrylic tubes slid through holes in the duct laid within the flow path. Depending on the specific region of the test section being measured, optics were placed into the one of the tubes. Optics within the tube collimated the incoming beam and created a light sheet in the direction of the test section.

2.5: Optics Table

In order to house the equipment necessary for PIV, a large sliding optical table was designed. PIV equipment on the table included an Nd-Yag Double Pulsed Laser, two LaVision Imager Pro-X CCD cameras, and an assortment of optical stands and rails. The base was constructed using 8020 aluminum extrusions, and held two Linos Rails connected to a Newport IG breadboard via four Linos Sliders as shown Figure 2–19. Use of an optical breadboard allowed for a variety of optical arrangements to be used on the organized 1'' in grid pattern.

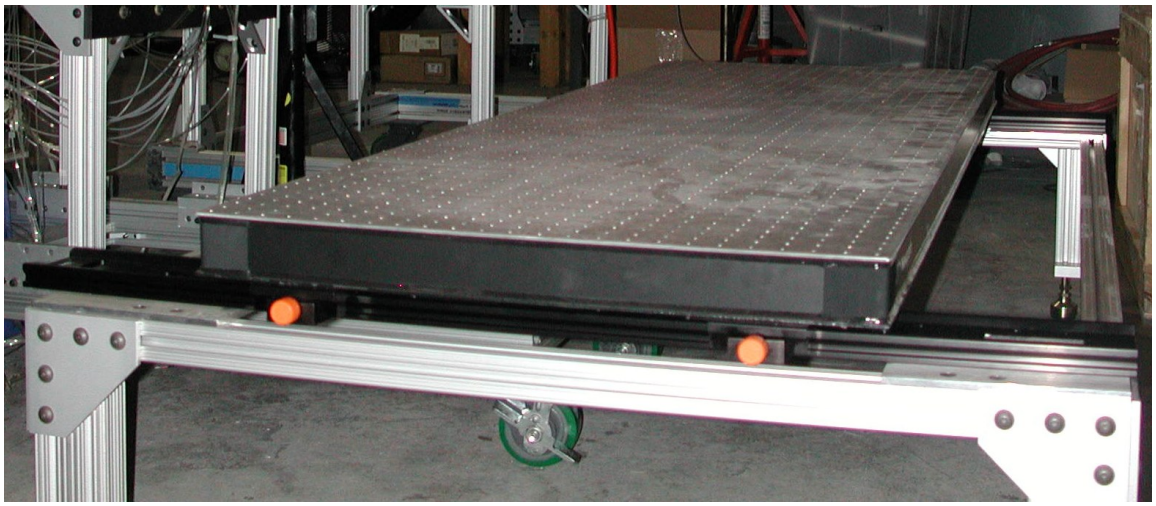

Figure 2–19: The sliding ability of the optic table allowed for calibration of the PIV system outside the tunnel.

The grid pattern was especially helpful during the laser alignment process. The ability to slide the optical table precisely with the PIV equipment was an important design criterion due to the inability to calibrate the PIV system inside the tunnel. A 12'' by 12'' Type 31 Calibration plate was used to calibrate the LaVision DaVis software outside the tunnel as it was too large to put into the test section.

The CCD Cameras were attached onto Manfrotto 410 camera rotation mounts, and connected to Linos carriages as shown in Figure 2–20. The rotation stands allowed the cameras to be tilted in the x, y, and z planes. The Linos carriages allowed the cameras to translate horizontally, and the optical rails allowed for both cameras to be translated vertically. Variability of the camera positions allowed for the collector field of view to be changed based upon the location data was being taken.

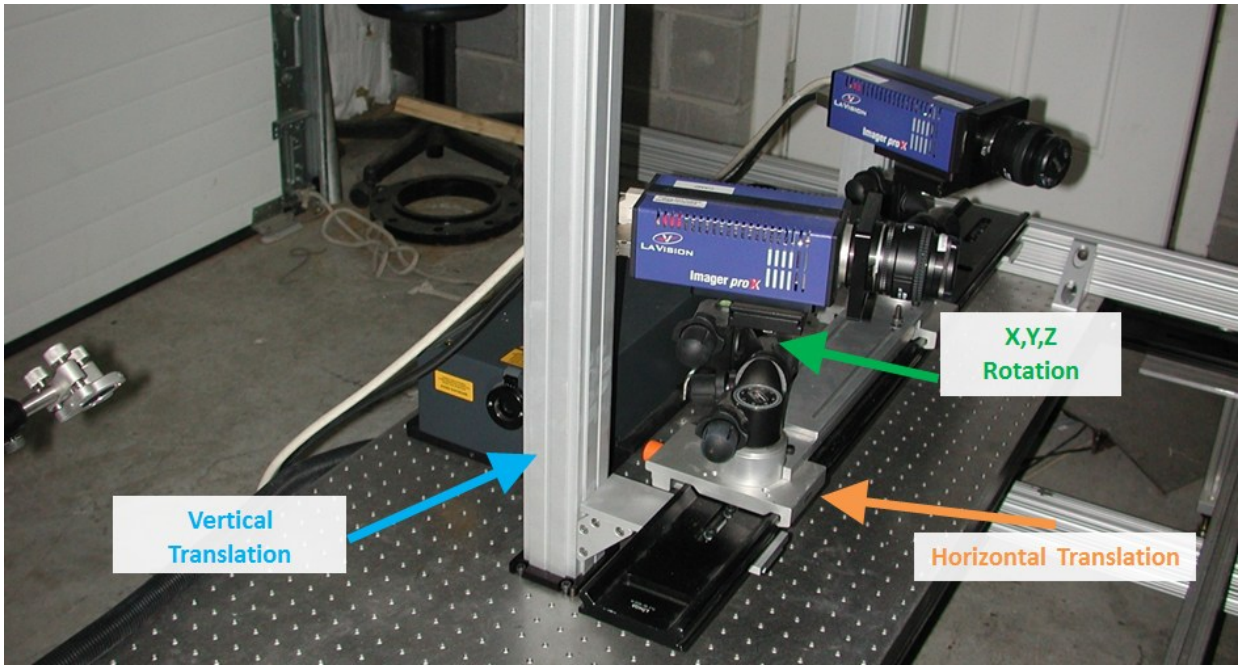

Figure 2–20: The optical table holds the CCD Cameras has the ability for rotation and translation in several directions.

Chapter 3 Instrumentation, Data Acquisition & Data Processing

Before obtaining PIV data, the flow conditions in the diffuser-collector were checked. Dimensionless numbers calculated in the test section need to match the values in the production model that characterize its flow. Some of these characteristic values would include inlet Mach number, inlet Reynolds Number, pressure recovery, and turbulence intensity. A three-hole probe, a boundary layer probe, a kiel probe, a hot film probe along with a range of static pressure taps helped obtain these values. Details of the instrumentation, the accompanying data acquisition components as well as processing methods used can be found below.

3.1: Temperature Measurement

A k-type thermocouple placed in the pressure tanks was used to obtain the value for total temperature. As the pressure tanks emptied during the run, the measured total temperature would drop over time. A linear fit was used for total temperature when calculating instantaneous Mach number, viscosity, and density. Temperature values were recorded at 800 Hz, and averaged over a window of four points resulting in a 200 Hz signal using Labview.

3.2: Diffuser Inlet Measurements

3.2.1: Pressure Measurements

Several pressure measurements were taken to characterize the flow entering the diffuser. A ring of six equally spaced static pressure taps around the case of the diffuser inlet were used to observe circumferential uniformity. To define the inlet Mach number and overall pressure recovery, total pressure was taken with use of a traverse and a three-hole probe at the six positions shown in Figure 3–1. An image defining the diffuser inlet plane can be seen in Figure 2–12 and Figure A4 of Appendix A.

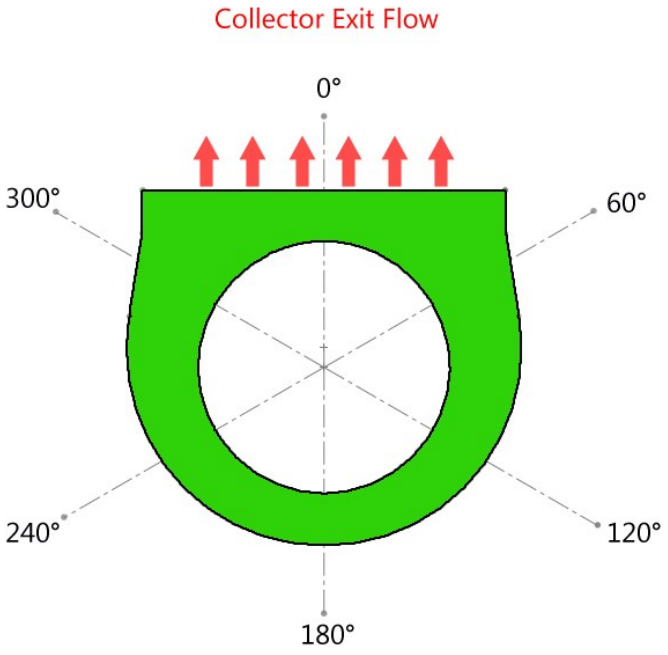

Figure 3–1: Circumferential locations for traverse measurements relative to the test section. A simplified front section view looking upstream shows the outline of the collector geometry.

Six slots located on the instrumentation ring acted as mounting positions for a traverse. The traverse allowed for precise point wise measurements of the inlet flow. Holes located on the case of the diffuser inlet allowed a 3/16'' probe to traverse into and out of the flow. A WAC – 187 three-hole wedge probe from United Sensor was used to gather total pressure, static pressure, and swirl angle from the three pressure values measured. Along the annulus height, time averaged data was gathered at ten points for each of the six positions. Ideally a single traverse run could be used to obtain the annular profile at one circumferential position; however artificial fluctuations would appear in the data when traversing at a high speed during a run. Once data for all six positions were taken, the measurements were combined and linearly interpolated to create a representative inlet diffuser flow. The point wise measurements were then used to determine a mass averaged total pressure and static pressure. Mass averaged values were used to calculate the inlet Mach number, inlet Reynolds number, and pressure recovery.

Although the three-hole probe was successful in obtaining the point wise measurements for the majority of the annulus, another probe needed to be used to obtain values near the hub and case. The specific geometry of the wedge probe only allowed measurements 0.20'' from the hub wall. To capture the total pressure profiles of the boundary layer on the hub and case a small profile boundary layer probe was traversed at the 180º position. Boundary layer data was then used to determine the diffuser inlet blockage value.

A kiel probe was also traversed tangentially into the flow as an approximate circumferential measurement. A circumferential measurement at mid annulus gathered total pressure data that was used to determine if wakes from the swirl vanes were present in the inlet flow. Both total pressure and static pressure were connected to a Scanivalve ZOC17 pressure scanner, which allowed for measurements to be recorded at 200 Hz using Labview.

3.2.2: Turbulence Intensity

Turbulence intensity values were obtained at the 180° position by traversing a hot film probe into the flow. Equipment for the hot film system included a Dantech type 55M91 Constant Temperature Anemometry unit, a TSI IFA-100 signal conditioner, and Nicolet BE256-LE high speed DAQ system. Hot film probe data was taken at ten points over the annular height identical to the three-hole probe measurements, but data was recorded at 100 kHz using the Nicolet system. To avoid aliasing, the TSI system was used to filter signals above 40kHz. An offset was also applied to keep the measured hot film voltages in range for the Nicolet system. Team256 software was then used to transfer voltage data from the Nicolet to a computer to be processed.

The recorded voltage data was processed with Matlab, which would take several steps to output a correlated velocity and the turbulence intensity. Typically, hot film processing involves taking measurements in a known flow field to determine a probe coefficient. This coefficient could later be used in the calculation process to relate the voltage values measured in an unknown flow field to determine velocity. For our setup an in-situ calibration was done using point wise static pressure and total pressure data obtained from previous traverse measurements. Holmberg's one-point calibration methodology was used to obtain a calibration coefficient. [Holmberg 1996]. The calculated coefficient then defined a relationship between Nusselt number and Reynolds number which was used to determine velocity. Note that a notch filter was used to remove large erroneous frequency components from the voltage signal at approximately 9855 Hz and 34550 Hz.

3.3: Diffuser Flow path Measurements

3.3.1: Circumferential Pressure Measurements

In addition to the inlet static pressure taps, several other circumferential measurements were taken at the diffuser exit. Six static pressure taps were equally spaced circumferentially on both the hub and case. The circumferential locations were identical to the positions of the traverse measurements, which allowed for easy evaluation. Comparing the circumferential uniformity between the diffuser inlet and exit would give notion to the impact of the collector on axial flow development.

3.3.2: Axial Pressure Measurements

Along with the taps mentioned above, a total of 66 taps were placed axially along the diffuser hub and case, as shown in Figure 3–2. The static pressures obtained from these values provided the rate of diffusion within the diffuser and were compared with the production model. At both the 0° and 180° positions on the hub, nine taps were placed axially and ten taps were placed axially at both positions on the case.

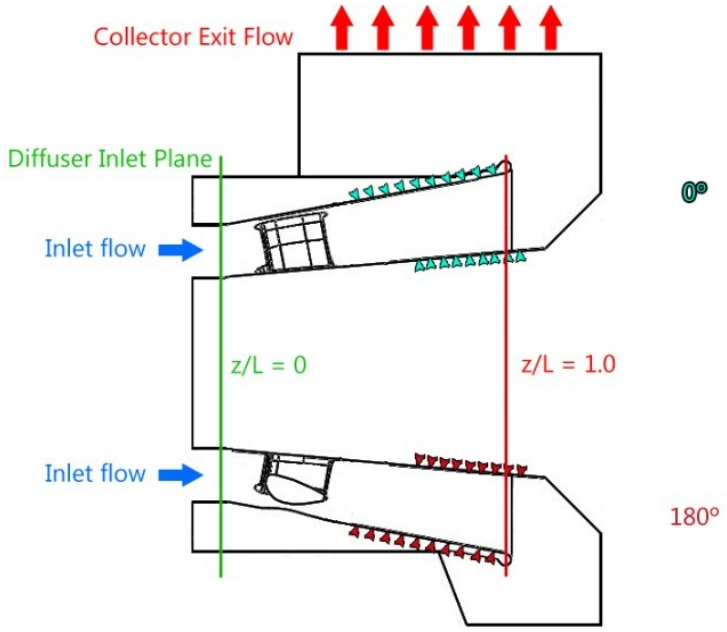

Figure 3–2: A simplified top section view of the test sections displays the array of pressure taps at 0º shown in blue, and the symmetric taps at 180º shown in red. Note that the strut orientation is not symmetric with the section view.

Twenty taps were circumferentially placed along the mid-pitch line in the strut passages that were closest to the 0° and 180° positions. Due to interfering geometry, taps in the struts of the diffuser could not be located exactly at the same positions. For each location five taps were put on the hub, and five were put on the case. Note that because the struts exhibit both lean and sweep, the positions for the 0° case taps were not at the exact circumferential location of the 0° taps on the hub. Similarly this occurred at 180° position as well. Figure 3–3 below shows a perspective view of the flow path where the 0° static taps can be seen. Static pressure taps were connected to a Scanivalve ZOC17 pressure scanner and used Labview to record values at 200 Hz.

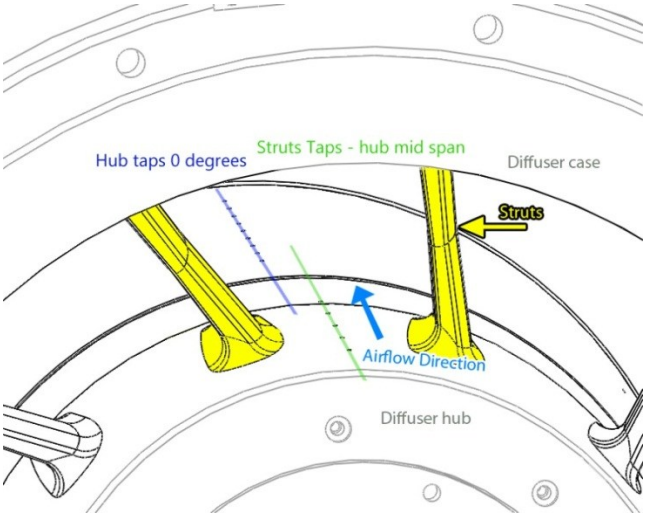

Figure 3–3: Looking downstream, a perspective view of the CAD model illustrates the lean and sweep of the diffuser struts, and the location of the strut pressure taps relative to the 0° position.

3.4: Collector Measurements

3.4.1: Pressure Measurements:

At the rectangular exit of the collector, 16 static pressure taps were equally spaced around the perimeter. The values obtained from the collector exit would indicate uniformity of the exiting flow, and were used to determine the overall pressure recovery of the diffuser-collector system.

3.4.2: PIV Measurements:

To observe the development of vortices from the diffuser exit, Stereo-PIV measurements were taken using the LaVision PIV system mounted on the optics table. Twelve slices of data were taken parallel to the collector back wall in order to reconstruct the three dimensional flow field. Figure 3–4 illustrates the PIV slices taken, and the restrictions due to limited viewing access and laser access. Viewing access was limited by the diffuser hub blocking the field of view, and laser access was restricted due to laser light impinging on the diffuser case.

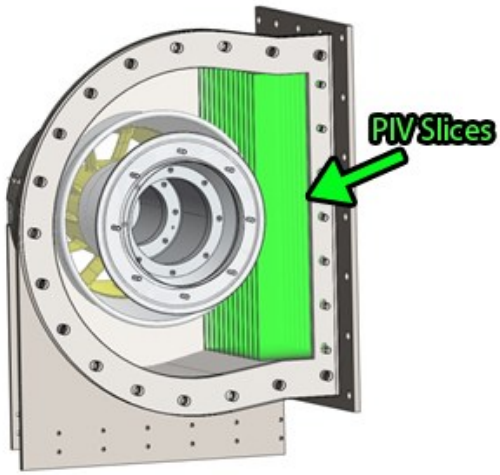

Figure 3–4: Twelve PIV slices used to reconstruct the three dimensional vortical structure developing through the collector system. Note that the laser sheet thickness has been enlarged, and the sheet travel has been shortened for this illustration.

The mean collector flow was obtained by taking 105 pairs of images at each of the twelve slices. By taking a large number of samples of the flow field, instantaneous flow structures would get averaged out and only leave the bulk flow. Each of the stereo images was first preprocessed using a sliding image filter to remove high intensity fluctuations due to reflecting laser light. DaVis software took the filtered images and was used to process and post process the velocity vector fields. A multi-pass technique for a 12 by 12 pixel center weighted interrogation area gave a dense vector field. The multi-pass technique shifted interrogation areas in order calculate velocity vectors with a higher correlation value. Next, spurious vectors were removed by using a median filter. This ensured that each calculated vector was within a specified range of its neighbors. Each of the 105 post processed vector fields were then combined using a threshold average. The threshold average would only average vectors in the field if it were common to at least 20% of all vector fields. Data in between each of the averages slices were linearly interpolated and plotted in FieldView for analysis.

3.5: Parameter Definitions

3.5.1: Inlet Mach Number Definition

Mach number for the diffuser inlet was determined using point wise traverse measurements of static and total pressure. Annular data from the six positions were then mass averaged and used to determine a single representative Mach number by means of Equation 3-1.

$$Ma^2 = \frac{2}{\gamma - 1}\left(\left(\frac{\overline{\overline{P_t}}}{\overline{\overline{P_s}}}\right)^{\frac{\gamma-1}{\gamma}} - 1\right) \qquad \text{Equation 3-1}$$

3.5.2: Inlet Reynolds Number Definition

Reynolds number was also used in the characterization of the diffuser inlet as defined by Equation 3-2. First static temperature was obtained using the calculated Mach number and the average total temperature. The static temperature was then used to determine density via the Ideal gas law, viscosity via Sutherland's law and then velocity from the speed of sound.

$$Re_{D_h} = \frac{\rho_{inlet} u_{inlet} D_h}{\mu_{inlet}} \qquad \text{Equation 3-2}$$

3.5.3: Pressure Recovery Definition

Pressure recovery was used to determine the overall efficiency of the diffuser-collector section using mass averaged static and total pressure at the diffuser inlet. Equation 3-3 defines pressure recovery as a comparison of the actual static pressure rise to the ideal pressure rise for the particular inlet flow. A local pressure recovery term, C_{pc}, can also be used by using the local static pressure at an arbitrary axial position as the exit in place of the collector exit static pressure.

$$C_p = \frac{\overline{P_{s,exit}} - \overline{\overline{P_{s,inlet}}}}{\overline{\overline{P_{t,inlet}}} - \overline{\overline{P_{s,inlet}}}} \qquad \text{Equation 3-3}$$

3.5.4: Static and Total Pressure Coefficient Definition

Values of total and static pressure were normalized by the inlet dynamic pressure for analyzing the diffuser inlet flow, as shown in Equation 3-4 and Equation 3-5. Inlet dynamic pressure was calculated using mass averaged total and static pressure determine from the traverse measurements. Note that the definitions for local pressure recovery and static pressure coefficient are identical. Local recovery was used in axial comparison of static pressure rise from the inlet, whereas static pressure coefficient was used in radial comparison of static pressure from the average value at the inlet.

$$P_s^* = \frac{\overline{P_{s,meas}} - \overline{\overline{P_{s,inlet}}}}{\overline{\overline{P_{t,inlet}}} - \overline{\overline{P_{s,inlet}}}} \qquad \text{Equation 3-4}$$

$$P_t^* = \frac{\overline{P_{t,meas}} - \overline{\overline{P_{t,inlet}}}}{\overline{\overline{P_{t,inlet}}} - \overline{\overline{P_{s,inlet}}}} \qquad \text{Equation 3-5}$$

3.5.5: Blockage Definition

A blockage term was used to compare the ideal volumetric flow rate to the actual flow rate. If flow is uniform and with a magnitude of the maximum velocity in cross section, then the entire area is being utilized to maximize flow rate. Reductions in flow rate due to non-uniformities of the velocity profile decrease the utilized area. This term is a ratio of the blocked annular area to the total area as defined in Equation 3-6 and Equation 3-7. The blockage term is an indication of a non-uniform velocity profile and therefore can also be an indication of the boundary layer displacement thickness.

$$A_B = \int^A (1 - \frac{u}{U}) dA \qquad \text{Equation 3-6}$$

$$B = \frac{A_{B,inlet}}{A_{inlet}} \qquad \text{Equation 3-7}$$

As mentioned previously, the geometric constraints of the three-hole probe did not allow for measurements near the hub or case. Extrapolated swirl distribution, extrapolated static pressure, and average total temperature were used to calculate the full annular velocity profile.

3.5.6: Kinetic-Energy-Flux Velocity-profile parameter Definition

As defined by Sovran and Klomp, this parameter is a ratio between the actual kinetic energy flux as compared to the minimum kinetic energy flux for a particular cross section.

$$\alpha = \frac{1}{A} \int^A \left(\frac{u}{u_{avg}} \right)^3 dA \qquad \text{Equation 3-8}$$

A truly uniform velocity profile would result in a flux parameter of one, whereas a non-uniform profile would calculate a parameter beyond unity.

Chapter 4 Experimental Testing & Results

To establish the conditions for the facility a tunnel shakedown process occurred prior to the evaluating the diffuser inlet flow. The shakedown process involved an iterative procedure between control valve variables, butterfly position and observing the resulting inlet conditions. Once flow was determined steady and representative of the production model, further data was taken. Details of the shakedown procedure, the annular inlet flow, and the axial characteristics of the diffuser can be found below.

4.1: Tunnel Shakedown

4.1.1: Obtaining Steady Conditions

To keep the flow conditions of the wind tunnel facility steady, the control valve would need to be opened at a rate relative to the pressure drop in the air storage tanks. It was known from previous tunnel shakedowns at the facility that the control valve needed to initially be opened to a large value. As the pressure dropped in the tanks from the initial opening, the opening percentage of the control valve was changed using a quadratic fit. Total pressure obtained mid height at the diffuser inlet during each run was used to indicate if the flow was changing with time. By tweaking the coefficients of the quadratic equation, a steady flow was finally found when the total pressure standard deviation during the steady part of the run was approximately 0.094 psi or a P_t^* of ±0.03. During this process it was also found that tunnel conditions took approximately 5.5s to reach a steady value.

4.1.2: Obtaining Accurate Inlet Flow Conditions

The facility had been determined steady; however the diffuser inlet conditions were not yet characteristic of the production model. The butterfly valve downstream from the collector exit was used to backpressure the facility and would in turn change the inlet Mach number. The butterfly valve was initially 90% open for safety concerns and was incrementally closed until the average inlet Mach number reached a value near the desired 0.420. Note that this desired Mach number is a mass averaged quantity. During tunnel shakedown an isentropic Mach number was calculated using the inlet circumferential static taps and a total pressure probe located mid height in the annulus. It was found that a 55% open butterfly valve gave approximately the correct Mach number but did not achieve the 1.940×10^6 Reynolds number. A total pressure of 29 psi at the diffuser inlet was calculated from the facility scaling; this was used as a guiding point to achieve the correct Reynolds number. Further modifications of the control valve opening rate would tweak the inlet total pressure and allow us to achieve an isentropic Mach number of approximately 0.417, and a Reynolds number of approximately 1.935×10^6; percent errors of 0.58% and 0.33% respectively. Annular data for the diffuser inlet was taken at these conditions and was used to determine a mass averaged Mach number of 0.413 and a Reynolds number of 1.939×10^6. Comparing the actual and ideal mass averaged diffuser inlet conditions, a percent error of 1.52% was calculated for Mach number and 0.05% for Reynolds number.

4.2: Diffuser Inlet Profile

Approximate values for the two major dimensionless characteristics for the test section had been achieved. However, the velocity profile and the swirl distribution for the diffuser still needed to be checked. The three-hole probe was traversed at the six circumferential positions in order to obtain the mass averaged circumferential distribution shown in **Figure** 4–1.

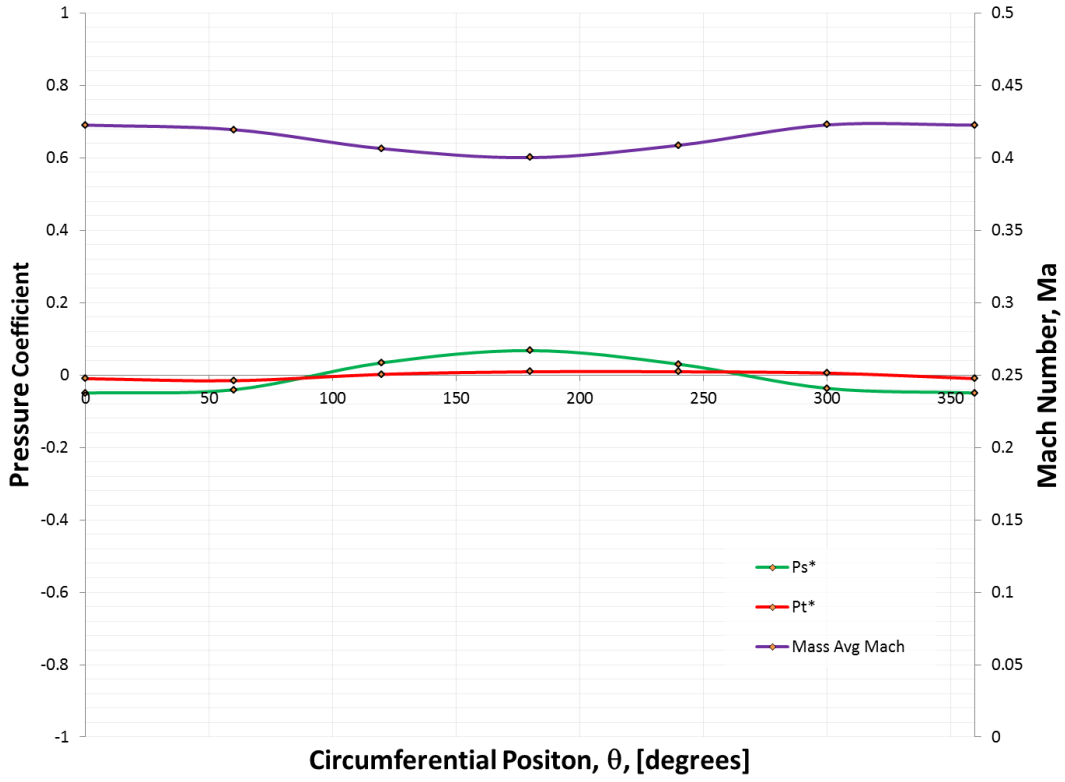

Figure 4–1: Circumferential distribution of pressure coefficient using mass averaged total pressure and static pressure, with a comparison to the Mach distribution

Initially it was thought the entire diffuser inlet profile would exhibit axisymmetric behavior. Yet when comparing the Mach distribution circumferentially, shown in Figure 4–1, one could see some slight variation. Total pressure coefficient was axisymmetric, while trends in static pressure coefficient agreed with the circumferential Mach distribution. Flow at the 0° position was approximately 5.45% faster than the flow at the 180° position. The pinched side of the collector, 180°, was expected to have much slower flow but at a position closer to the diffuser exit. It seems that once the collector flow had developed, slowed regions of flow would propagate back into the diffuser. Regions of flow all around the collector had this same backing effect creating the circumferential profile seen. The cause of these slowed regions and hence the backing effect may be due to the particular geometry of the collector.

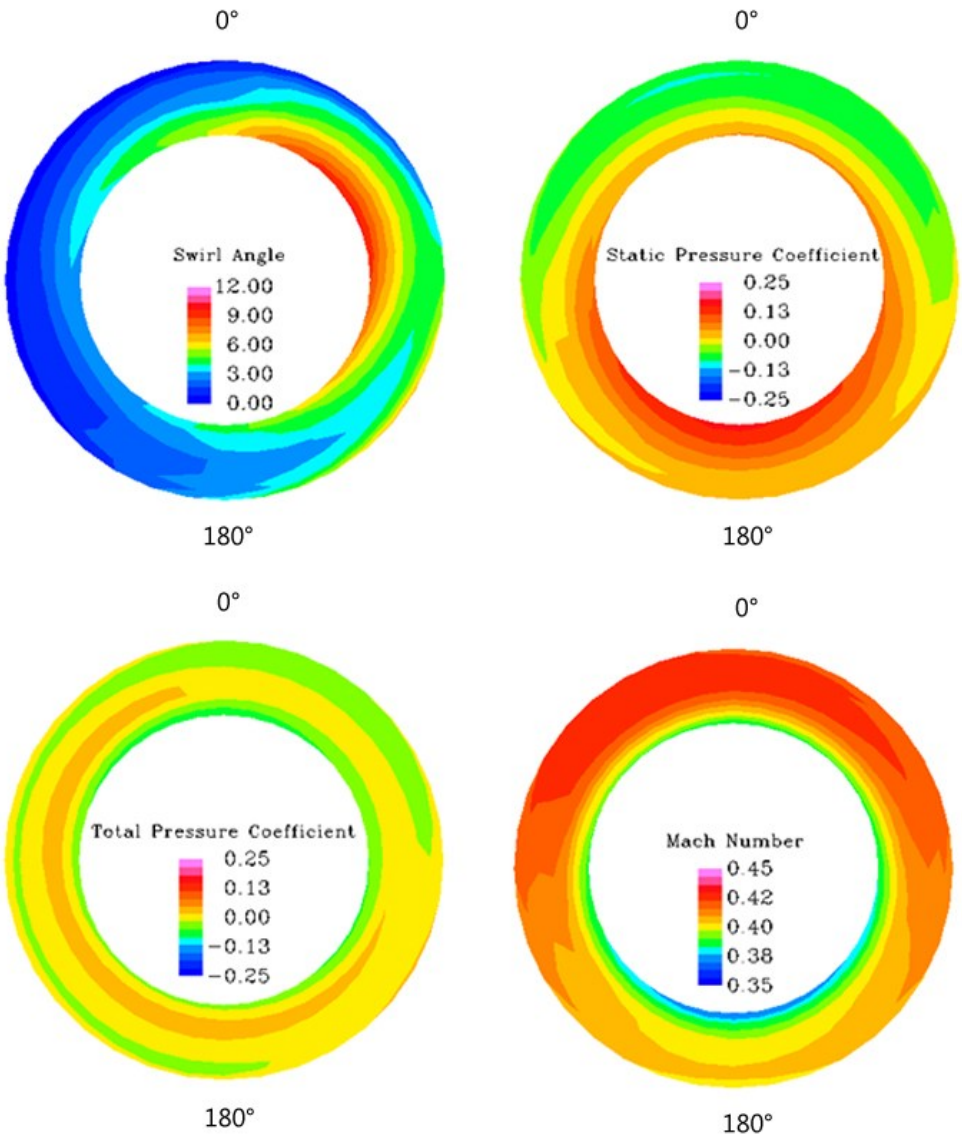

Figure 4–2: Contour plots of the inlet annular flow showing Mach number, swirl angle, static pressure coefficient, and total pressure coefficient. Data was interpolated between the six positions.

Figure 4–2 shows the swirl distribution over the annulus showed the general trend of increasing swirl from case to hub. The intended swirl distribution followed this same characteristic; however the swirl was expected to be in the range of 5º to 10º with an average swirl near 7º. Swirl seen throughout the entire annulus was slightly smaller with an average swirl of approximately 4º. This lower average swirl may have been due to turbulence grid being placed too close to the swirl vanes, and reducing their overall impact. The annulus also showed a strong circumferential distribution that was quite interesting. Regions of higher swirl were located near 60º and regions of lower swirl were found near 240º, forming a mirror-like image about the pinched section of the collector. The cause of the circumferential swirl distribution is unknown and requires further investigation.

The radial Mach number distribution showed expected behavior with a relatively uniform profile from hub to case; varying by only 4.5%. Flow on the hub side was slightly slower as intended. Faster flow on the case was ideal as it helped to delay separation. An image of the radial Mach distribution at 180º is shown later in Figure 4–3 for further clarification.

The static pressure coefficient between each of the six positions also followed the same relative patterns, exhibiting a gradual rise when going from case to hub. The rise in static pressure was expected, as it agreed with the designed Mach distribution. The total pressure coefficient was anticipated to be axisymmetric as well as relatively flat in the annulus. Drops near the hub and case were expected due to losses in the boundary layer. The total pressure annular data agreed with the expected result, however to quantify the boundary layer a blockage term was used.

4.3: Diffuser Blockage

Extrapolated three-hole probe data along with boundary layer measurements were used to obtain **Figure** 4–3.

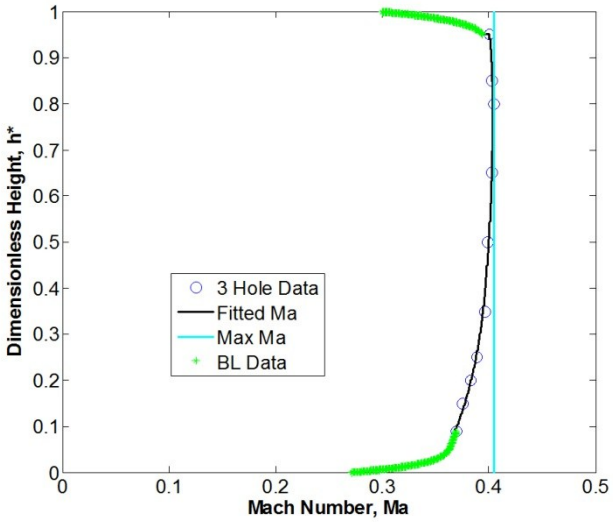

Figure 4–3: The diffuser inlet axial Mach distribution shows non uniformity from hub to case, with expected drops near the annulus walls

Using Matlab to process the axial Mach profile, a blockage value of 2.97% was determined. This blockage fraction was in the expected range and was slightly higher than the 2% used in Sovran & Klomp's annular diffuser characterization. A larger blockage was expected because of Sovran & Klomp's use of a uniform velocity profile as compared to the non-uniform velocity profile seen in **Figure** 4–3. This blockage value was important as it would allow for comparison of the current test section with the optimum geometry lines determined by Sovran & Klomp. From previous studies it was known that higher blockage values tended to reduce pressure recovery for typical diffusers, therefore a slightly lower pressure recovery was anticipated for the test section [Stevens & Williams 1980].

A displacement thickness of 0.03'' or approximately 1.5% of the annulus height can be calculated using Equation 4-1. An assumption of an equivalent boundary layer on both the hub and case is used.

$$B = \frac{2\delta^*}{h}$$ Equation 4-1

4.4: Inlet Turbulence Intensity Profile

The turbulence intensity profile for the annulus at the 180° position was expected to be in the range of 4 to 6%. This value was based upon the turbulence grid design and the distance away from the grid itself. The production model diffuser encountered turbulence intensities between 5 to 6%. The turbulence intensity at the diffuser inlet was important as it would affect the mixing of the fluid and hence the diffusion. Figure 4–4 shows that the turbulence intensity was in the projected range. The distribution from hub to case showed a general increase in intensity near the hub, with the lowest values near the case. Higher turbulence intensity values up to approximately 8% tended to increase pressure recovery for a particular diffuser geometry, therefore hub pressure recovery was expected to be larger [Hestermann 1995].

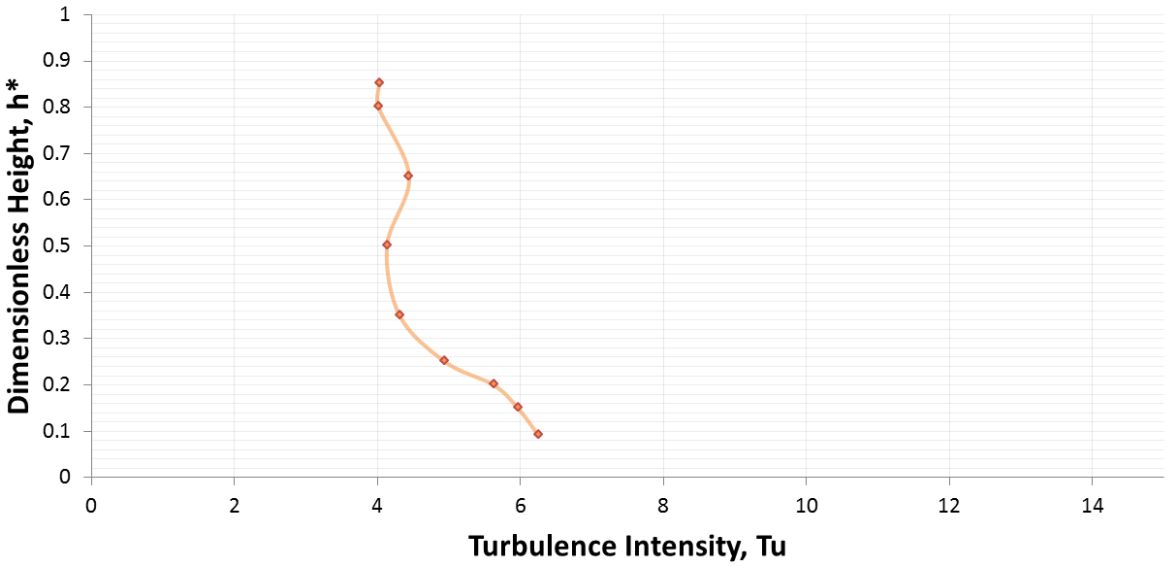

Figure 4–4: Turbulence intensity values obtained at the 180º position showed a slight increase towards the hub.

4.5: Local Pressure Recovery Distribution

It was known that many variables would contribute to pressure recovery in the diffuser. Some of these variables would include the diffuser geometry, Mach number, swirl distribution, the presence of struts, blockage, and the inlet turbulence intensity. An assortment of axial taps at the 0º and 180º positions were used to obtain the axial pressure distribution. Pressure recovery was observed throughout the diffuser section on both the hub and case as shown in Figure 4–5, and Figure 4–6.

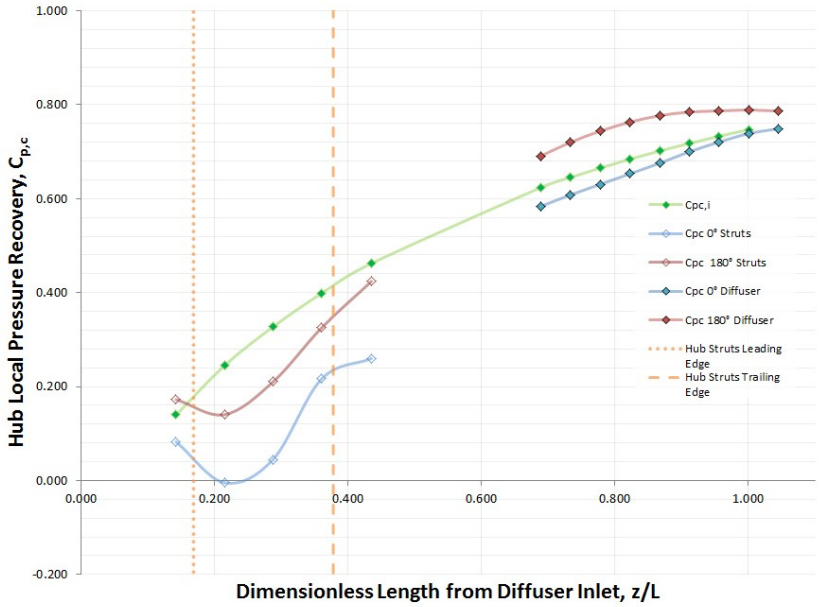

Figure 4–5: Local pressure recovery on the hub over the diffuser axial length

Local pressure recovery on both the hub and case were expected to increase over the axial length and eventually level off near the diffuser exit. As shown above the local pressure recovery did follow our anticipated results with a few small exceptions. An initial drop due to flow acceleration through the diffuser strut passages was observed. The ideal local pressure recovery based upon the annular area ratio was plotted in green; note that this does not account for the reduced area due to the struts. With the initial assumption of axisymmetric flow, pressure recovery lines were expected to be analogous between the two positions. Near the diffuser exit at 180º a slight drop in recovery was a possible indication of separation. Faster flow at the 0º position lead to a slight decrease in local recovery [Thayer 1971].

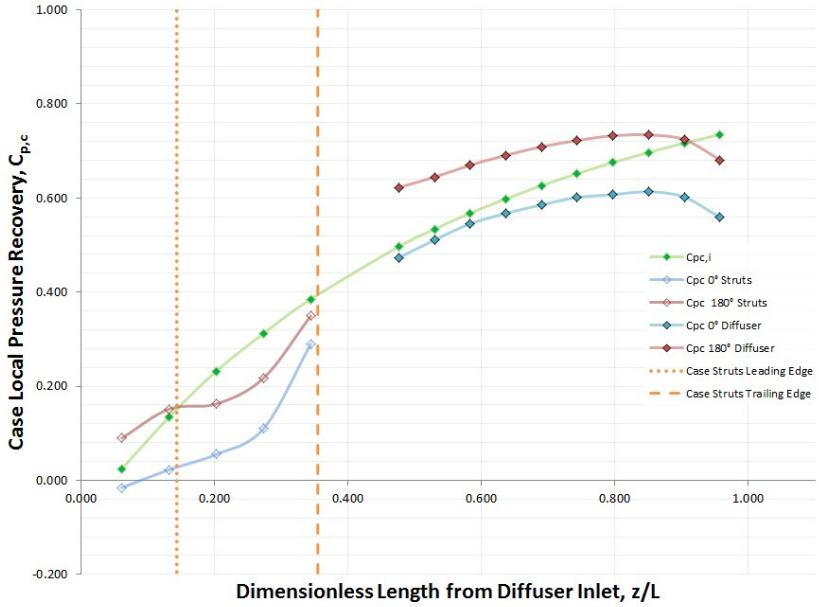

Figure 4–6: Local pressure recovery on the case over the diffuser axial length

Case local pressure recovery followed the same general trends. Local recovery values on the case were typically smaller than the corresponding values of local recovery on hub near the same axial position. This general tendency for more efficient diffusion on the hub was due to the combination of annular velocity distribution, higher turbulence intensity, and geometric parameters. Near the exit of the diffuser case the recovery values started drop significantly indicating a possible reacceleration of flow into the collector.

Pressure recoveries from the diffuser exit to the collector exit were considerably different. Circumferential data at the diffuser exit gave an average local recovery on hub of 0.72, while average case recovery was 0.54. Static pressure measurements at the exit of the collector showed uniformity, however the calculated pressure recovery for the diffuser-collector subsystem was only 0.52. This large drop in recovery can be attributed to two different effects. The first potential effect was inefficient diffusion as a result of the collector geometry. The second effect was losses due to the development the complex collector flow. The PIV section below contains details of the collector flow development.

4.6: Collector Stereo-PIV Results

Stereo-PIV data in the collector was combined using FieldView resulting in the figures below. Velocities were normalized by mass averaged velocity at the diffuser inlet. Due to time constraints, only data in the regions of 0º to 90º, and 270º to 360º were collected. Poor seeding on the bottom quadrant during PIV measurements resulted in discontinuous data sets between 0º to 90º, as shown in Figure 4–7. Although seeding was not ideal in the upper right quadrant, the data was found to be symmetric with major structures seen between 270º to 360º.

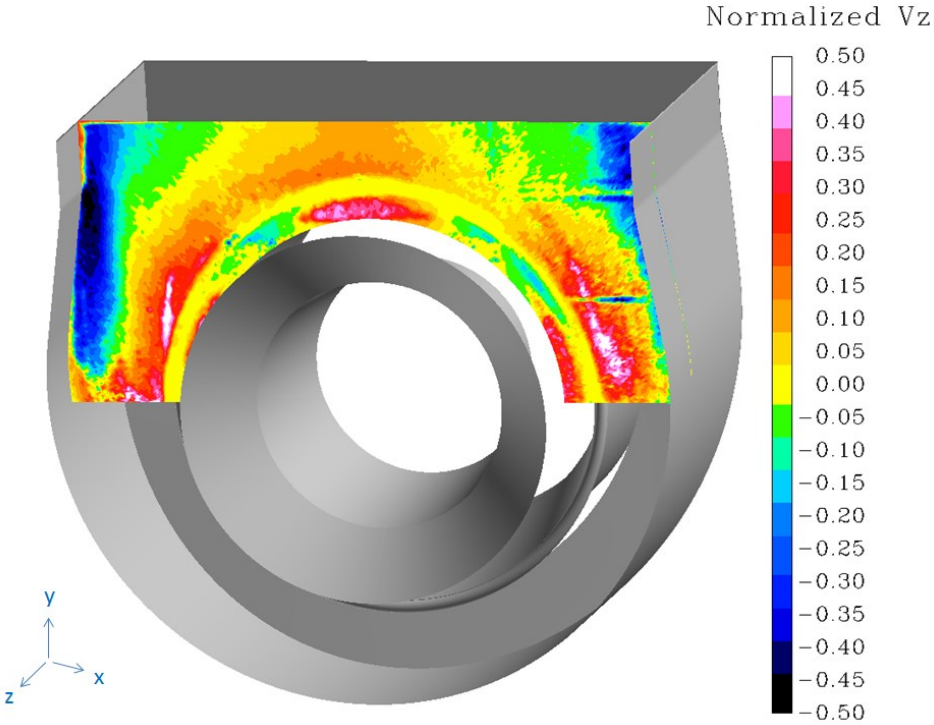

Figure 4–7: Flow two inches from the diffuser exit, contains high velocity regions impinging on the rear wall of the collector. Positive z direction defined as flow out of the page, parallel to the collector rear wall.

Normalized velocity in the z direction indicated high velocity regions leaving the diffuser while also causing entrainment of the flow behind the diffuser case. Along the collector side walls flow is seen traveling towards the collector front wall indicating a vortex type structure. Velocities decreased proportionally as they moved closer to the collector exit. The decreasing trend seen could relate to vortex strength decaying as it moved to regions of larger area. The significant amount of entrained flow at the 90º and 270º positions combined with the small area may have increased the strength of the vortex during its formation.

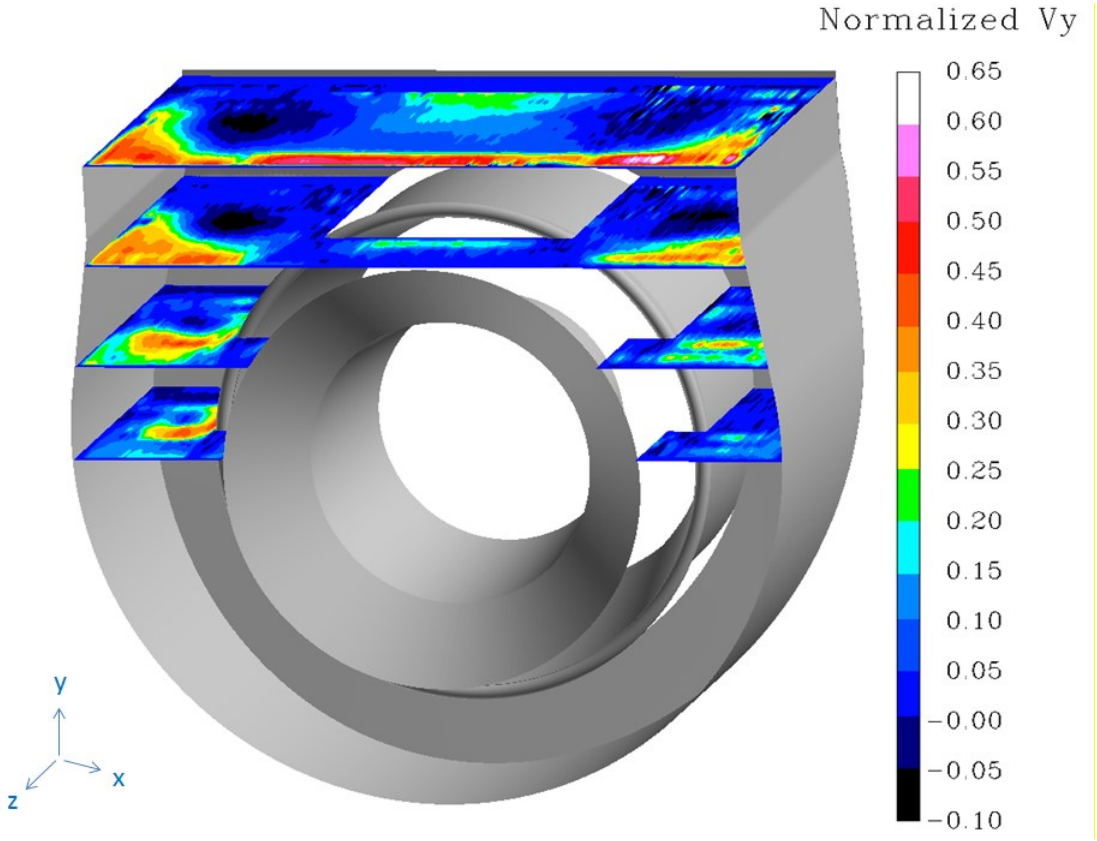

Figure 4–8: Several planes cut parallel to the collector exit show the growth of vortical structures over the flow path. Normalized Vy was plotted, where positive Vy represents flow exiting the collector.

Several planes cut parallel to the exiting flow in

Figure 4–**8** show the development of the two anticipated vortical structures in the collector. As expected both vortical structures were symmetric about the center of the collector. Each of the structures was quite large, encompassing the majority of the collector exiting flow. Normalized Vy velocities for flow leaving the collector was on average near 0.11, with a maximum of 0.55. A kinetic-energy-flux velocity parameter of 9.27 was calculated at the collector exit as compared to the ideal value of one. The calculated parameter signified that there is great amount of kinetic energy that diffuser-collector subsystem could still convert into static pressure rise.

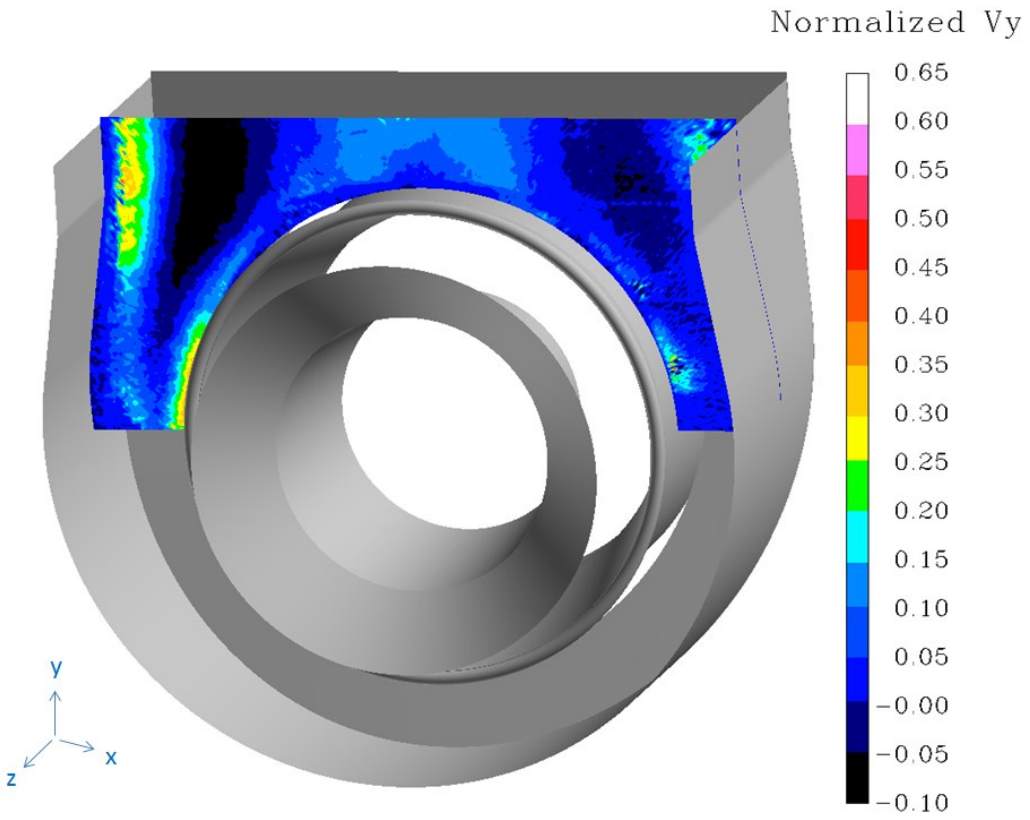

Figure 4–9: The reversed flow region of the vortex core grew with collector geometry. At the collector exit both cores represented nearly 15% of the exiting area.

Looking at the planes of data in Figure 4–8, the movement of the vortices core toward the front wall of the collector can be seen as well. As the space in the collector expands the structures shift and grow accordingly. Angular movement of the vortex cores was approximately 18º as compared to the 21.2º opening of the collector front wall. Growth of vortices cores in the y direction can be more clearly visualized in Figure 4–9. Both vortex cores contained reversed flow, when combined was representative of 15% of the exiting collector area. Flow near the vortice cores was near stagnant while regions of high velocity were near the collector walls. In both the y and z directions large velocity gradients were found near created the collector walls allowing for potential loss due to shearing effects.

Chapter 5 Conclusions & Recommendations

5.1: Conclusion

A subsonic wind tunnel facility was designed and built in order to evaluate flow within a quarter scale diffuser-collector subsystem. The wind tunnel facility utilized a blow down configuration and was able to match both Mach number and Reynolds number for the subsystem within 2% error. Mass averaged conditions during testing were 0.418 for Mach number, and 1.939×10^6 for Reynolds number at the diffuser inlet. A flow conditioning section prior to the test section was used to obtain the necessary swirl distribution, velocity distribution, turbulence intensity, and boundary layer thickness. Swappable components within the flow conditioning section would allow for variation of each of the critical flow parameters. Variation in the flow conditioning section could be used in future experiments to study the effect of turbine operating conditions on the diffuser-collector subsystem.

Traverse measurements were taken at the diffuser inlet in order to verify that conditions representative of design operation. Several pressure measurements were also taken within the diffuser and at the collector exit to evaluate the efficiency and basic characteristics of the subsystem. Developing flow within the collector was then observed through the use of Stereo-PIV.

Pressure data taken throughout the subsystem indicated inefficiencies caused by the collector. A large amount of the diffusion within the subsystem occurred within the diffuser resulting in local pressure recovery in the range of 0.47 to 0.78. The overall pressure recovery defined by the collector exit was significantly lower, and was determined to be 0.52. Reduced recovery at the collector exit was presumed to be a combination of the particular collector geometry creating regions of loss as well as inefficient diffusion. Large regions of complex flow were result of the collector geometry and were found to affect the flow conditions up to the diffuser inlet.

Stereo-PIV data showed the development of two large counter rotating symmetric vortices through the collector. High velocities gradients were also found near the collector walls where the vortices developed. The impinging vortices along the wall, and size of the vortices themselves allowed for potential total pressure losses within the collector. As the geometry of the collector changed, the path and size of each of the vortices would change accordingly. Together the vortices contained the majority of the collector and created significant regions of reversed flow affecting the diffusion.

The design and testing of this facility was used as a baseline assessment for future projects, as well as an initial evaluation of the collector diffuser-collector subsystem. The facility was found to be successful in achieving the desired goals for the project. Recommendations for future tests with this facility are discussed below.

5.2: Recommendations

Several recommendations are listed below in an attempt to improve facility design, future experimentation, and diffuser-collector efficiency

5.2.1: Facility Design changes and improvements:

- The collector made of sheet metal was cost effective and rigid, however dimensions were inaccurate and resulted in difficult assembly. A segmented collector made of anodized aluminum would be suggested for future models.
- Creating more access doors or windows throughout the facility would allow for quick and easy maintenance as well as use of flow visualization techniques
- Use of an access duct made of clear cast acrylic. This would allow observation of the exiting vortical structures using a simple Stereo-PIV setup. Laser access and optical access through the duct with additional laser access in the collector rear wall.
- Swirl vanes made of another rapid prototyping material capable of being machined. The particular material chosen was quite inaccurate in comparison to the adjoining flow path components.
- Reduce uses of radially located bolts. During assembly it was difficult to connect parts radially using the tight tolerances necessary for an annular test section.
- Total pressure measurements throughout the diffuser and collector section to identify high loss regions.

5.2.2: Potential improvements to diffuser-collector efficiency

- Changes in the collector geometry to reduce impact of the vortices. More specifically increase distance from the diffuser exit to the collector rear wall. This should to allow the vortex pairs to expand with the same relative energy [Bernier 2011]. The same energy expanded over a larger area could reduce any potential losses within the collector and reduce the impact on the diffuser flow.
- Use of guide vanes or a curved rear collector wall to promote flow in the exiting direction. This could potentially minimize vortex development and improve efficient diffusion.
- Trips incorporated into the diffuser struts to increase turbulence intensity levels within the diffuser. This could reduce potential separation within the diffuser and improve diffusion.

References

Anderson, J. D. (2008). *Introduction to Flight.*

Barlow, J. B., Rae, W. H., & Pope, A. (1999). *Low-Speed Wind Tunnel Testing.*

Bell, J. H., & Mehta, R. D. (1988). *Contraction Design for Small Low-Speed Wind Tunnels.* Washington, DC.: National Aeronautics and Space Administration.

Bernier, B. C. (2011). Impact of a collector box on the pressure recovery of an exhaust diffuser system. *ASME Turbo Expo.* Vancouver.

Dryden, H. L., & Schubauer, G. B. (1947). The Use of Damping Screens for the Reduction of Wind-Tunnel Turbulence. *Journal of Aeronautical Sciences, 14*(4), 221-228.

Finzel, C., & Casey, M. V. (2011). Experimental Investigation of geometric parameters on the pressure recovery of low pressure steam turbine exhaust hoods. *ASME Turbo Expo 2011.* Vancouver.

Hestermann, R. (1995). Flow field and performance characteristics of combustor diffusers: a basic study. *Journal of engineering for gas turbines and power, 117*(4), 686-694.

Hoffman, J. (1981). Effects of Free-Stream Turbulence on Diffuser Performance. *Journal of Fluids Engineering, 103*(3), 385-390.

Holmberg, D. G. (1996). *A Frequency Domain Analysis of Surface Heat Transfer/Free-Stream Turbulence Interactions in a Transonic Turbine Cascade.* Virginia Polytechnic Inst. and State Univ., Blacksburg.

Japikse, D., & Baines, N. C. (1998). *Diffuser design technology.*

Japikse, D., & Pampreen, R. (1978). Annular Diffuser Performance for an Automotive Gas Turbine. *Journal of Engineering for Gas Turbine and Power, 101*(3), 358-372.

Liu, J., Cui, Y., & Jiang, H. (2003). Investigation of flow in a steam turbine exhaust hood With/Without turbine exit conditions simulated. *Journal of Engineering for Gas Turbines and Power, 125*(1), 292-299.

Liu, J.-J., & Fu, J.-L. (2011). Unsteady interactions between axial turbine and nonaxisymmetric exhaust hood under different operational conditions. *Journal of Turbomachinery, 134*(4).

Lowe, T. K., & Simpson, R. L. (2009). An advanced laser-Doppler velocimeter for full-vector particle position and velocity measurements. *Measurement Science & Technology, 20*(4).

Pietrasch , R. Z., & Seume, J. R. (2005). Interaction between struts and swirl flow in gas turbine exhaust diffusers. *Journal of Thermal Science, 14*(4), 314-320.

Prandtl, L. (1933). The Attainment of a Steady Air Stream in Wind Tunnels. *NACA-TM-726*.

Ragni, D., Schrijer, F., Scarano, F., & Oudheusden, B. (2011). Particle tracer response across shocks measured by PIV. *Experiments in fluids, 50*(1), 53-64.

Roach, P. (1987). The generation of nearly isotropic turbulence by means of grids. *International Journal of Heat and Fluid Flow, 8*(2), 82-92.

Sovran, G., & Klomp, E. D. (1965). Experimentally determined optimum geometries for rectilinear diffusers with rectangular conical or annular cross-section. *Fluid Mechanics of Internal Flow*.

Stevens, S. J. (1980). Influence of inlet conditions on the performance of annular diffusers. *Journal of fluids engineering, 102*(3), 357-363.

Thayer, E. (1971). Evaluation of curved- wall annular diffusers. *ASME Pap 71-WA/ FE-35.*

Ubertini, S., & Desideri, U. (2000). Experimental performance analysis of an annular diffuser with and without struts. *Experimental Thermal and Fluid Science, 22*(3-4), 183-195.

Yoon, S., Stanislaus, F. J., Mokuly, T., Singh, G., & Claridge, M. (2011). A Three-Dimensional Diffuser design for the retrofit of a low pressure turbine using in-house exhaust design system. *ASME Turbo Expo 2011.* Vancouver.

Zhang, W., & Paik, B. G. (2007). Particle image velocimetry measurements of the three-dimensional flow in an exhaust hood model of a low-pressure steam turbine. *Journal of Engineering for Gas Turbines and Power, 129*(2), 411-419.

Appendix A: Modifications & Simplifications to the Test Section

The model used in the Techsburg experimental setup only required the essential flow features; therefore, a large amount of detailed geometry from the Solar Turbine model was deemed irrelevant for the Techsburg model. Using *Solidworks,* the Solar Turbine model was uniformly scaled to one fourth of the true scale. Changes for the Techsburg Model were made to avoid scaling issues, and to accommodate instrumentation are discussed below in detail.

A1: Simplification & Neglected Geometry

In order to simplify the geometry only necessary flow features were used. A large portion of the Solar Turbine model included mounting points on the case and hubs which were changed based upon the upstream and downstream components in the experimental facility.

The production diffuser-collector section is subject to high temperatures and the provided model included expansion joints in the metal due to heat expansion. One of these gaps along the diffuser-collector annulus can be seen in Figure A-1. Because the experimental setup would only be exposed to moderate room temperatures, these gaps were simplified to continuous sections.

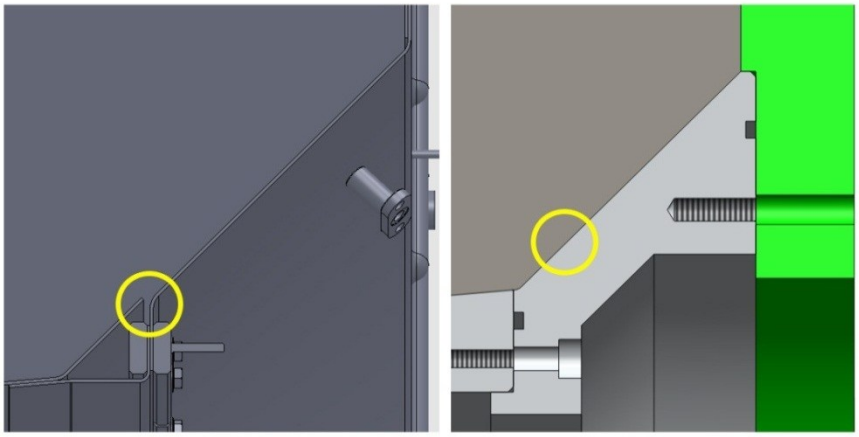

Figure A-1: a) Small gaps along the annulus were in the Solar Turbine model. b) Gaps were made continuous in the experimental model due to testing conditions deeming them unnecessary

A2: Modifications due to Scaling Issues

When scaling a model down, material thicknesses and clearances can often become unreasonably small. In our case this issue only occurred at two locations, one near the exit of the diffuser flow path on the diffuser casing, and another on the collector near the bleed pipe.

A2.1: Diffuser Case Web Thickness

The scaled thickness of this web is approximately 0.04 inches. Consultations with the head of our machine shop lead to an increase in web thickness to approximately 0.25 inches as shown in Figure A-2. The thickness was large due to the manufacturing process used to shape this web, and it would insure structural stability of the part.

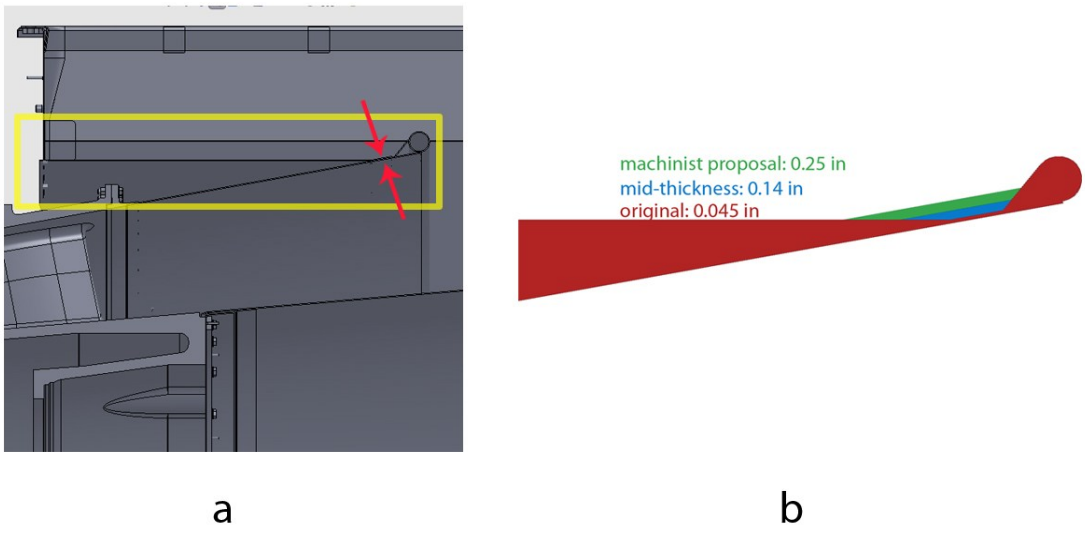

Figure A-2: a) The thickness of the web in the Solar CAD Model b) Suggested thicknesses for the part

A2.2: Bleed Pipe Hole Location

Another area which was changed due to the scaling issues was the location of the bleed pipe hole in the collector. In the experimental setup a 90° elbow was attached to the bleed pipe hole from the outside of the collector. The attached elbow created an interference with the upstream diffuser case flanges, and therefore the bleed pipe hole position was changed by 1.25'' as shown in Figure A-3.

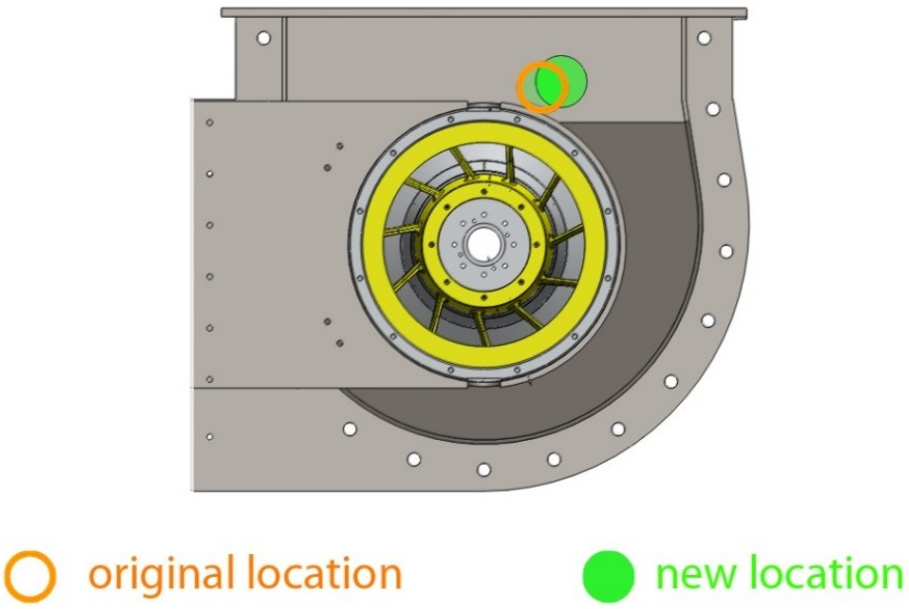

Figure A-3: Bleed pipe hole was moved 1.25 inches at 20° avoid geometric interferences

A3: Modifications for Instrumentation

In order to obtain various flow quantities for the analysis of the diffuser-collector section, the model was modified to accommodate instrumentation. Details regarding the specific modifications are found below.

A3.1: Modifications to obtain Pressure data at the Diffuser Inlet Plane

In the experimental setup measurements are taken at several locations. Data measured from the diffuser inlet plane can be used to calculate diffuser efficiency terms such as the pressure recovery coefficient. Ideally the instrumentation plane would lie coincident with the diffuser inlet plane to best characterize the diffuser section.

In order to achieve the desired instrumentation plane the diffuser was extended upstream axially. Note that the actual flow path geometry has not changed; a joint was simply translated axially. Figure A-4 illustrates the changes made to the diffuser in order to achieve the ideal inlet plane; the axial position of the diffuser inlet plane is represented with a green line.

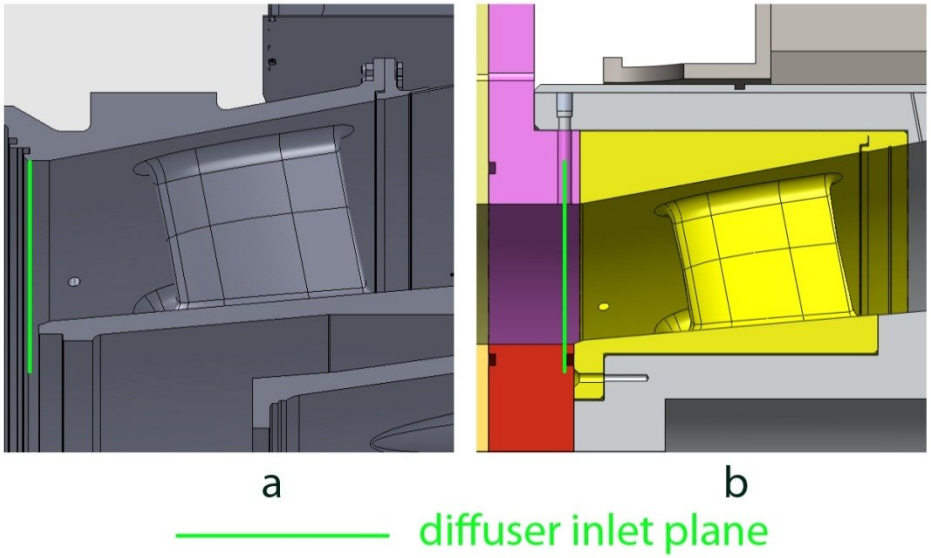

Figure A-4: a) Diffuser inlet plane in Solar Model b) Diffuser inlet plane in experimental model

A3.2: Modifications for Static Pressure Measurements

To take the data necessary for analysis of the diffuser-collector section many pressure taps were placed along the flow path.

On the diffuser casing two wide channels were machined to allow for pressure tubing to lay beneath the surface as shown in Figure A-5. Before testing the channels were filled with an epoxy material and covered with electrical tape to simulate the true geometry of the diffuser case and avoid any flow path discontinuities.

Figure A-5: Machined channels were filled with epoxy to minimize any possibility of extraneous instrumentation in the flow

Similarly another channel was made for pressure taps located circumferentially along the diffuser exit plane. An image of this circumferential channel can be seen in Figure A-6.

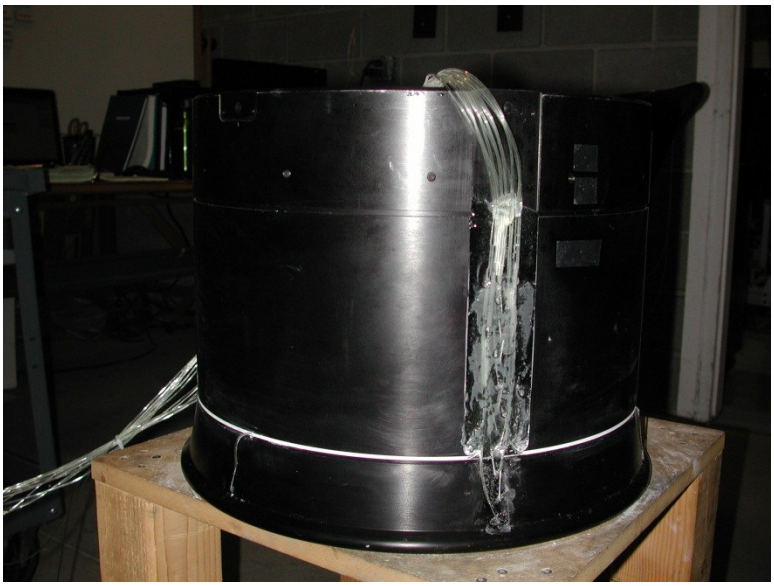

Figure A-6: The circumferential channels were filled with joint compound which created a continuous flow path

A3.3: Modifications for PIV Windows

Two windows were put into the diffuser-collector section to allow for PIV measurements. The rear wall plate of the collector was made out of an acrylic material to allow viewing access for the PIV cameras as shown in Figure A-7. Cell Cast acrylic material was used because it is a strong material with optical properties suitable for camera viewing access. The flow path geometry of the front plate window stays the same, and therefore would not affect the flow.

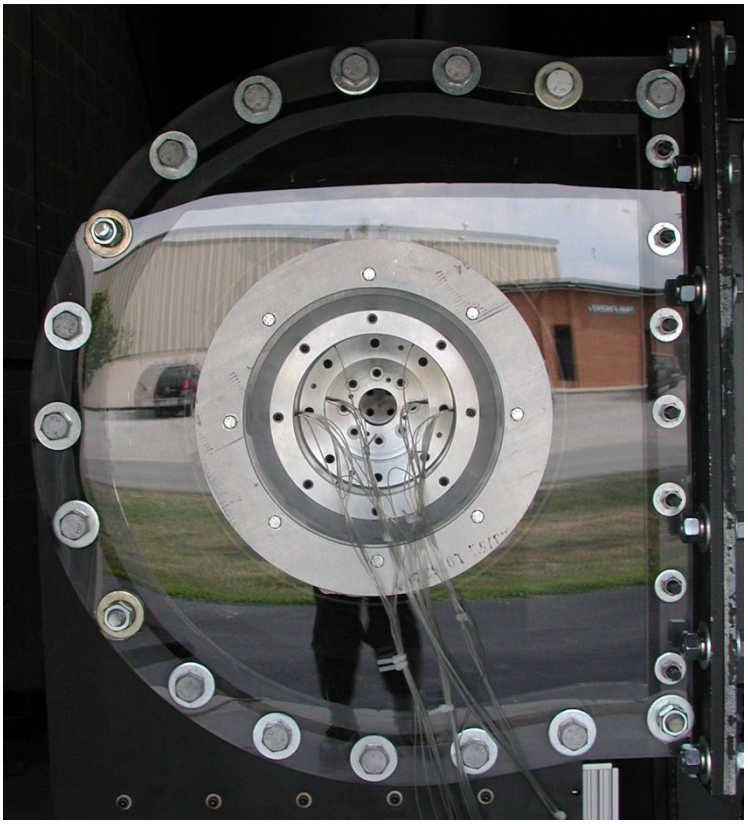

Figure A-7: Viewing access of the acrylic rear wall plate using the Techsburg facility orientation

Experimental setups involving PIV often have the problem of seeding build up on the viewing surface. To avoid this issue the acrylic front plate was designed to slide in and out of the collector shell for maintenance purposes.

Another small window was designed to slide into the collector shell at the apex of the collector curve. This small window, shown as green in Figure A-8, allows for a laser sheet to illuminate the collector flow in the image quadrants nearest to the collector apex. The shape of this window created a small flat in the flow with a maximum deviation of approximately 0.061 inches from the original flow path.

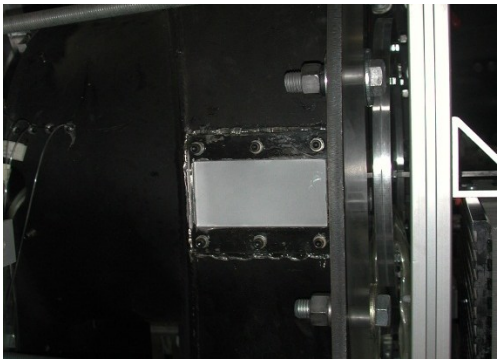

Figure A-8: Perspective showing the small acrylic window used for PIV

Appendix B: Uncertainty Calculations

The section below covers uncertainty values for the major parameters discussed in the results section. In Table B-1 values of instrumentation uncertainty can be seen for the pressure and temperature measurements taken. Uncertainties for Mach, temperature, velocity, and pressure recovery are calculated based upon the instrumentation uncertainty.

Measurement	Instrument	Uncertainty
Axial Static Pressure	ZOC 17 Pressure Scanner 5psid	± 3.25E-03 psi
Inlet Static & Total Pressure	ZOC 17 Pressure Scanner 15psid	± 9.75E-03 psi
Total Temperature	Omega TAC80B k-type Thermocouple to Analog Converter	± 6.1°F

Table B-1: Various instrumentation uncertainty values

Equations B-1, B-2, B-3, and B-4 were used to calculate the uncertainty for Mach number, static temperature, velocity, and pressure recovery. Values of uncertainty would propagate from initial parameters to later parameters. For example, uncertainty from Mach number and total temperature would propagate into the static temperature because static temperature was a function of both Mach number and total temperature.

$$\delta Ma = \sqrt{\left(\frac{\partial Ma}{\partial P_t}\delta P_t\right)^2 + \left(\frac{\partial Ma}{\partial P_s}\delta P_s\right)^2} \qquad \text{Equation B-1}$$

$$\delta T_s = \sqrt{\left(\frac{\partial T_s}{\partial T_t}\delta T_t\right)^2 + \left(\frac{\partial T_s}{\partial Ma}\delta Ma\right)^2} \qquad \text{Equation B-2}$$

$$\delta u_{in} = \sqrt{\left(\frac{\partial u_{in}}{\partial T_s}\delta T_s\right)^2 + \left(\frac{\partial u_{in}}{\partial Ma}\delta Ma\right)^2} \qquad \text{Equation B-3}$$

$$\delta C_p = \sqrt{\left(\frac{\partial C_p}{\partial P_{t,inlet}}\delta P_{t,inlet}\right)^2 + \left(\frac{\partial C_p}{\partial P_{s,inlet}}\delta P_{s,inlet}\right)^2 + \left(\frac{\partial C_p}{\partial P_{s,meas}}\delta P_{s,meas}\right)^2} \qquad \text{Equation B-4}$$

An estimated uncertainty was calculated for PIV measurements using Equation B-5 and Equation B-6. Since mean flow was being observed it was a safe assumption that uncertainty in velocity was largely dependent upon sample size rather than instrument uncertainties [Lowe 2009].

$$\delta V_{piv} = \frac{\sigma_{piv}}{\sqrt{N}} \qquad \text{Equation B-5}$$

$$\delta V_{norm} = \sqrt{\left(\frac{\partial V_{norm}}{\partial u_{in}}\delta u_{in}\right)^2 + \left(\frac{\partial V_{norm}}{\partial u_{in}}\delta u_{in}\right)^2} \qquad \text{Equation B-6}$$

Table B-2 shows the values of uncertainty calculated for major parameters used in data analysis. Percentage uncertainty was also calculated for each of the parameters and it showed that pressure measurements had uncertainties less than 1%. As expected SPIV measurements showed large uncertainties of approximately 1% for the in plane velocities x and y. The out of plane velocities, z component, showed even larger uncertainties on the order of 2% which was also anticipated.

Characteristic Parameter	**Calculated Uncertainty**
Diffuser Inlet Mach Number	± 0.001
Static Temperature	± 3.28 K
Diffuser Inlet Velocity	± 0.113 m/s
Pressure Recovery	± 0.002
Collector PIV Normalized Velocity	V_x: ± 0.01 V_y: ± 0.01 V_z: ± 0.02

Table B-2: Calculated uncertainty values for major parameters